JÜLICH Forschungszentrum

HAW HAMBURG

Master Thesis

Development of an automated, microcultivation and analytical workflow for screening of peroxygenase producing *K. phaffii* strains

09.06.2023
Philipp Dante Zinn, matriculation number: █████

Supervising tutor (HAW Hamburg): Prof. Dr. Gesine Cornelissen
Supervising tutor (Forschungszentrum Jülich): Prof. Dr. Marco Oldiges

University of Applied Sciences Hamburg
Department Life Sciences
Course of Studies Biotechnology

In cooperation with:
Forschungszentrum Jülich
Institut für Bio- und Geowissenschaften (IBG)
Biotechnologie (IBG-1)

Table of contents

1. Abstract

Bioprocess development has seen significant advancements in recent years, with a strong emphasis on automation to improve efficiency, productivity and to accelerate research. This thesis aimed to contribute to this field by developing an automated microcultivation and analytical workflow for the screening of peroxygenase producing *Komagataella phaffii* strains.

The analytical workflow consists of an automated ABTS assay which demonstrated its robustness and consistency in determining the activity of the target enzyme, providing a crucial parameter for the screening process. Furthermore, the workflow allowed for automated measurement of protein concentrations via Bradford assay, aiding in the evaluation of peroxygenase expression levels. The results indicated that the automated assays were reliable and provided reproducible data. The target enzyme, peroxygenase, is regulated by a PDF promotor which is repressed in the presence of carbon sources such as glycerol or glucose. Hence, methanol is used to provide carbon for the protein biosynthesis of POX by taking advantage of the methanol utilization pathway and the PDF promotor of the engineered *Komagataella phaffii strain*. However, challenges were encountered in the production of peroxygenases in BioLector® microcultivations, requiring further investigation.

The aim of the overlying EnzyPol project is to apply peroxygenase as a substitute for cobalt in curing of unsaturated polyester resins as a more sustainable, environmentally friendly and renewable alternative.

This work contributes to the ongoing efforts in bioprocess development and demonstrates the benefits of lab-scale automation. By successfully developing an automated workflow for analysing POX activity, this thesis lays the foundation for high-throughput screening of POX producing *Komagataella phaffii* strains and optimal process parameters.

2. Introduction

In recent years the growing demand of novel biotechnological products, such as biopharmaceuticals, vaccines, and enzymes led to an increasing importance of robust and fast bioprocess development [1,2]. Numerous steps including cell line development, optimization of media components and fermentation conditions as well as choosing the ideal downstream processing methods are involved in the development of such processes. To reduce the time-consuming and labour-intensive nature of bioprocess development, many steps can be automated while also improving the efficiency, accuracy, and reproducibility. This results in faster development times, reduced costs, and higher product yields. Automation refers to the use of advanced technologies such as robotics, high-throughput screening, and artificial intelligence, which help to streamline and optimize bioprocess development workflows, allowing researchers to quickly identify the optimal conditions for cell growth, product yield and efficacy [3–7]. As demonstrated in Figure 1, small-scale cultivation and lab automation increase process insight and control while still maintaining a high experimental throughput in contrast to conventional bioprocess development [6].
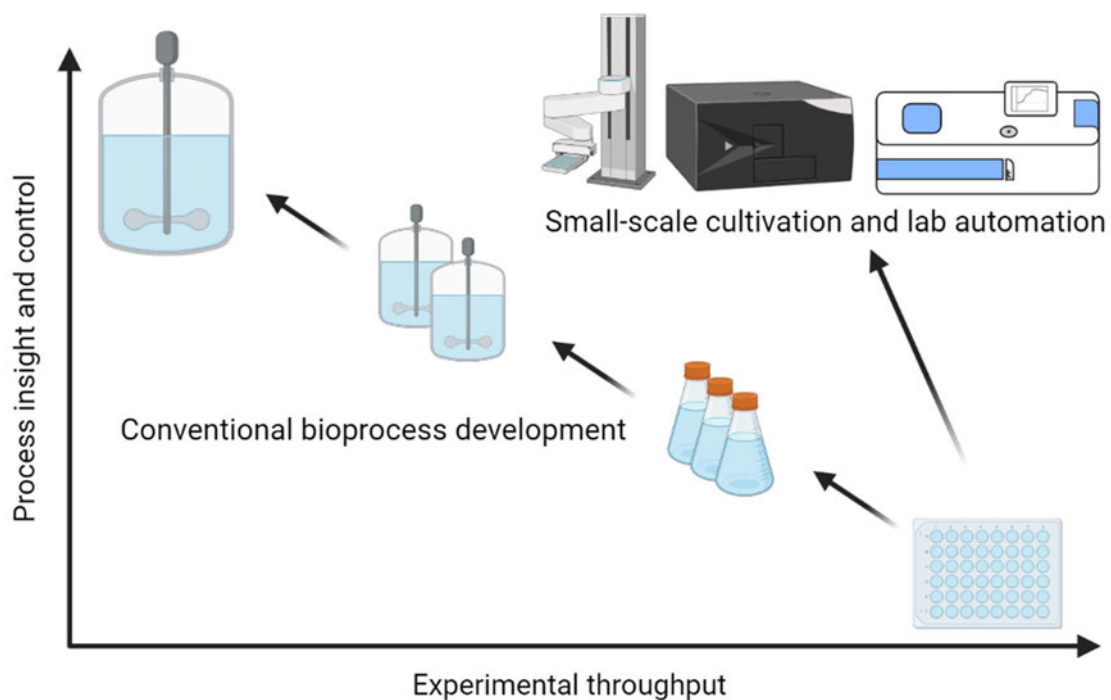
Figure 1: Small-scale cultivation and lab automation allow high process insight and control while maintaining relatively high experimental throughput compared to conventional bioprocess development. (Based on Hemmerich et al. (2018))

The objective of this thesis is to develop and validate an automated screening workflow including parallel microscale cultivation, protein quantification and determination of enzymatic activity. To set this workflow up, fungal peroxygenases were selected as the target protein produced by *Komagataella phaffii* (formerly classified as *Pichia pastoris*) as the model organism.

In the following chapters, the overlying EnzyPol project will be outlined, then, the organism *Komagataella phaffii* and the methanol utilization pathway will be elaborated. Next, the ABTS assay, which measures enzymatic activity as well as the Bradford assay, which quantifies the protein concentration will be explained. Afterwards the BioLector® system will be described and, lastly, the experimental approach is presented.

2.1. EnzyPol Project

EnzyPol is a subproject of the competence center Bio4MatPro, which is part of the Bioeconomy Model Region in the Rhenish Mining Area funded by the Federal Ministry of Education and Research (BMBF). This subproject aims to discover an industrially applicable, enzymatic alternative to cobalt curing of unsaturated polyester resins [8].

Cobalt curing refers to the process of using cobalt-based compounds as accelerators to initiate the chemical reaction that cures or hardens composites, such as unsaturated polyester resins used in fiberglass-reinforced plastics. This process involves mixing cobalt compounds with the resin and then exposing the mixture to air, which triggers the curing process [9]. This material is widely used in the construction of vehicles, boats, and wind turbine rotor blades [10].

However, the use of cobalt comes with numerous downsides like its carcinogenic properties, its hazardous mining conditions and limited availability [11,12]. Because cobalt is also used in lithium-ion batteries for electric vehicles, a significant increase in demand is expected, leading to a high risk of cobalt shortage by the year 2050 [13]. The EnzyPol project aims to find a substitute catalyst with equivalent performance. Biotechnologically produced enzymes are a promising alternative to replace cobalt with numerous advantages such as their renewable and biodegradable characteristics [14]. Finding such an alternative

to cobalt required identifying, testing, and optimizing enzymes based on specific application criteria. The project will also focus on developing and optimizing microbial production processes for these enzymes and conducting economic evaluations of the substitute material through application testing [8].

The BYK-Chemie GmbH, an associate of the EnzyPol project, conducted a proof-of-concept study, showing that horseradish peroxygenase (HRP) can be used as a substitute for cobalt in the curing process. However, HRP is only available in very limited amounts (~1 kg per year) [unpublished data from BYK-Chemie GmbH]. For an industrial scale, it was decided to produce fungal peroxygenases in *Komagataella phaffii*.

2.2. Fungal peroxygenase

Fungal peroxygenase (POX) are a class of enzymes found in fungi that are involved in the degradation of lignocellulosic materials, such as wood and plant biomass. These enzymes are oxidoreductases and can catalyse a variety of reactions, including the oxidation of organic compounds, cleavage of lignin, and the reduction of peroxides. The structure of fungal peroxygenases consists of a heme-containing active site that is surrounded by several amino acid residues. These residues play important roles in substrate binding and catalysis, and their composition varies depending on the POX type. The active site is capable of binding and activating hydrogen peroxide (H_2O_2), which is used as a co-substrate to oxidize organic substrates [15–17].

The oxidation reaction catalysed by fungal peroxygenases involves the transfer of an oxygen atom from H_2O_2 to the organic substrate, resulting in the formation of an unstable intermediate that can undergo further reactions to produce a variety of products. This mechanism is used to trigger the polymerization of a mediator in compound curing. The exact mechanism of this reaction is not yet fully understood, but it is believed to involve the formation of a high-valent iron-oxygen intermediate, which can abstract hydrogen atoms from the organic substrate [15,18].

The *Komagataella phaffii* strain used in this thesis is genetically modified to produce POX. The expression cassette of POX includes a promoter system engineering approach,

incorporating a PDF promoter [19,20] (a novel variant of the *Hansenula polymorpha* FMD promoter [21]). This promoter exhibits repression in the presence of carbon sources such as glycerol or glucose in the cultivation medium. However, it becomes derepressed once these carbon sources are depleted and its activity is further enhanced through the addition of methanol. This regulatory mechanism allows for tight control of gene expression and ensures that the promoter is active only when needed.

In order for *Komagataella phaffii* to successfully produce the target enzyme, it is necessary to utilize a carbon source that provides energy for POX production without repressing the PDF promoter. For this reason, the methanol utilization pathway is utilized.

2.3. *Komagataella phaffii* and the methanol utilization pathway

Komagataella phaffii (*K. phaffii*) is a highly popular organism in biotechnology due to its many advantages and the profound knowledge on industrial and academic cultivation and scale-up. It is simple to cultivate in inexpensive growth media, features well established post-translational modification techniques, has a high secretion capacity, and is considered safe as it has no known pathogenicity to humans or animals [22–24]. A key aspect of *K. phaffiis* popularity lies in the fact, that it is a methylotrophic yeast, inheriting strong methanol-inducible promotors derived from the methanol utilization (MUT) pathway. The initial reaction of the MUT pathway starts in the peroxisomes, thus, methylotrophic yeasts are used in studies regarding peroxisome biosynthesis and function, primarily used for recombinant protein production. The expression of the alcohol oxidase (AOX) gene, which encodes the first enzyme of the MUT pathway, is regulated by the alcohol oxidase I (AOX1) promotor. The promotors activity depends on the type and concentration of carbon source in the growth medium. Equally to the PDF promotor, the AOX1 promotor is repressed in the presence of carbon sources such as glycerol or glucose. In contrast to the PDF promotor, simple depletion of these carbon sources does not lead to activation of AOX1 in order to prevent the synthesis of alcohol oxidase and conserve cellular resources. Only when methanol is present, the AOX1 promotor is activated and the AOX gene is highly expressed, which leads to high levels of alcohol oxidase activity and efficient methanol utilization [19–21,24,25]. Thus, a typical cultivation profile for producing a recombinant protein involves a batch and fed-batch phase with focus on biomass

accumulation with glycerol or glucose as carbon sources. Hence, a starvation phase follows in which the remaining carbon source is depleted to derepress the PDF promotor and start POX production. Thereafter, an adaptation phase can be applied. Here, the process conditions are gradually changed from optimal cell growth to optimal protein production. Lastly, methanol is introduced to the cell to mediate the yeast to switch to the MUT pathway [23].

For this thesis, *K. phaffii* is used to produce POX after depletion of glycerol/glucose in combination with methanol as carbon source, taking advantage of the MUT pathway. Because POX is secreted into the cultivation medium, only simple downstream processes are needed. To evaluate the activity of POX, the ABTS assay was used.

2.4. ABTS Assay – Measuring enzymatic activity

The enzymatic ABTS assay is a common method used to measure the activity of enzymes, particularly peroxygenases. The assay is based on the oxidation of the ABTS (2,2'-azino-bis(3-ethylbenzothiazoline-6-sulfonic acid)) molecule by hydrogen peroxide in the presence of the tested enzyme. The oxidized ABTS now becomes a radical molecule, which can be measured photometrical due to its blue-green colour. The colour intensity of the product is directly proportional to the product formation and therefore enzymatic activity, measured at a wavelength of $405 - 415$ nm. The catalysed reaction can be seen in Figure 2.

2,2'-azino-bis(3-ethylbenzothiazoline-6-sulfonic acid)
[ABTS]
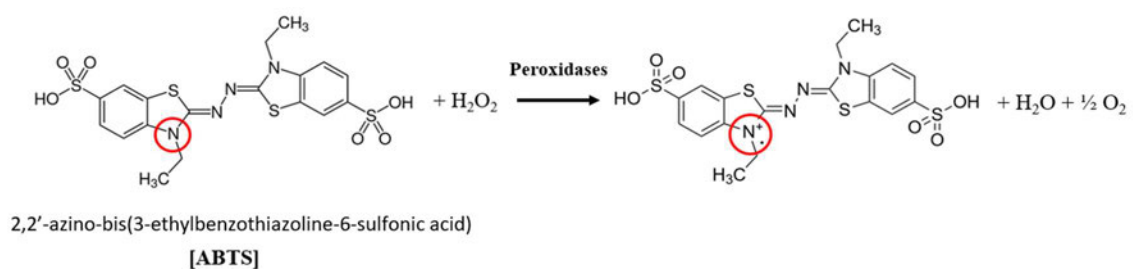
Figure 2: Chemical reaction of the ABTS assay. Peroxygenases mediate the oxidation of ABTS when H_2O_2 is present. ABTS is oxidised to a radical state, which leads to a blue-green product, photometrically measurable at 405-415 nm (see red circle) and 2 H_2O. The amount of oxidized ABTS is proportional to the enzymatic activity.

2.5. Bradford Assay – Measuring protein quantification

Protein quantification assays are crucial in biochemistry and molecular biology to determine the protein concentration of a sample. One of the most commonly used methods for protein quantification is the Bradford assay. The assay principle is based on the binding of the dye Coomassie Brilliant Blue G-250 to the amino acid residues of proteins. When the dye binds to the protein, it undergoes a shift in its absorption spectrum from 465 nm to 595 nm, resulting in a change in colour from brown to blue. The degree of colour change is directly proportional to the amount of protein that is present in the sample. The Bradford assay is performed by adding the protein sample to the Coomassie solution and measuring the absorbance at 595 nm using a photometer after incubation. A standard curve generated with samples of known protein concentrations allows to quantify the protein content of a sample of unknown concentration. The Bradford assay is simple, fast, and relatively insensitive to interfering substances. However, the assay is not specific to the target enzyme, as the total protein content of a sample is determined. Thus, it can only be regarded as a rough method for POX quantification.

2.6. BioLector® cultivation system

On one hand, shake flask cultivation is a simple and inexpensive method, providing basic information about growth and behaviour of microorganisms. However, the simplicity comes with downsides like inconsistent oxygen transfer and limited on- and at-line analytics. Lab scale fermentation on the other hand offers a more comprehensive view of the fermentation process, allowing for better control and monitoring of key variables such as dissolved oxygen (DO) and pH. However, lab scale fermentation is costly and only applicable with limited throughput due to intensive hands-on labor [26,27].

The BioLector® from Beckman Coulter GmbH is a high-throughput microfermentation system, designed for automated and parallel cultivation and monitoring of microbial cultures. The closed system of the multifermenter allows for oxygen regulation inside the cultivation chamber. The system operates with a multi-well plate containing up to 48 individual wells, each equipped with non-invasive, online optodes that provide real-time data on parameters such as DO, pH, and scattered light (backscatter) which is an indicator for biomass. The technique for online biomass measurement utilizes backscatter signals

of a specific wavelength to detect particles, including microorganisms, in the cultivation broth. A wavelength of 620 nm is employed to measure biomass concentration, with higher backscatter signals indicating higher biomass levels in the respective well. In order to assure accurate measurement, microtiter plates with transparent well bottoms, non-transparent base plates, and non-transparent well walls are required. This approach provides a valuable means of monitoring biomass dynamics throughout the cultivation process, offering insights into microbial growth and development [28]. A schematic representation of this can be seen in Figure 3.
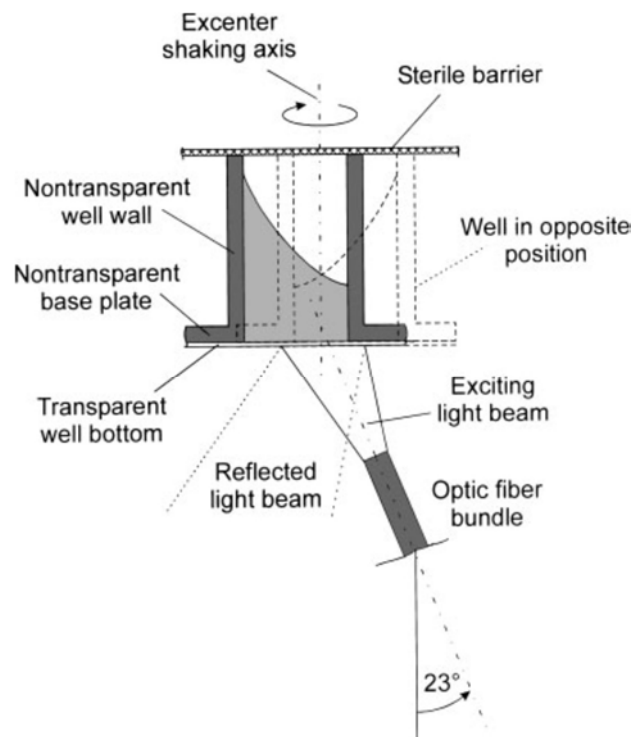
Figure 3: Scheme of the measurement device inside of the BioLector® (modified after Samorski et al., 2005)

There are different types of multi-well plates. The shape of the so-called FlowerPlate® works similarly to baffles in shake flasks and bioreactors, enabling higher shaking frequencies and increasing the gas-liquid mass transfer for a kLa up to 650 h^{-1} [29]. Another benefit is the special sealing film which consist of three layers. The bottom layer is a gas permeable membrane allowing gas transfer between the wells and the cultivation chamber of the BioLector®. The top layer is a silicone mat with a venting hole for gas exchange and a slit for each well. Repeated sampling and dosing can be performed trough the slit since it is self-resealing. The middle layer works as a bonding sheet for the bottom and top layer. A schematic illustration of the FlowerPlate® is illustrated in Figure 4.
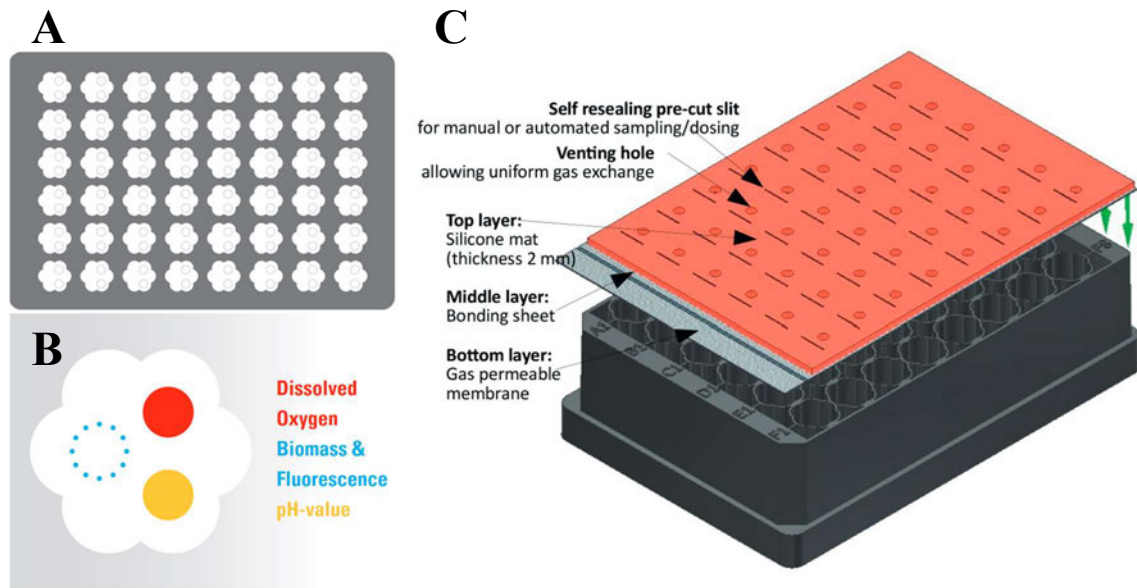
Figure 4: Schematic representation of the FlowerPlate® design from m2p-Labs. (A) On the bottom of each well are optodes for the DO, the pH-Value and a spot for biomass and fluorescence measurement. (B) FlowerPlate® design. (C) Sealing film consisting of a gas permeable membrane, a silicone mat, and a bonding sheet. (Source: https://www m2p-labs.com, last visited: 06.04.2023)

Another plate type is the microfluidic (MF) FlowerPlate®. Here, the wells of the first two rows of the plate serve as reservoirs for the respective columns below. The purpose of the reservoir wells can vary and contain *i.e.*, medium for a fed-batch cultivation, acid or base for pH-control, or an induction solution such as methanol. Membrane valves on the microfluidic chip are controlled pneumatically, to pump liquids through independent microchannels into each cultivation well. Constant, linear, or exponential feeding profiles can be applied. An illustration of this plate type can be seen in Figure 5.

A   **B**
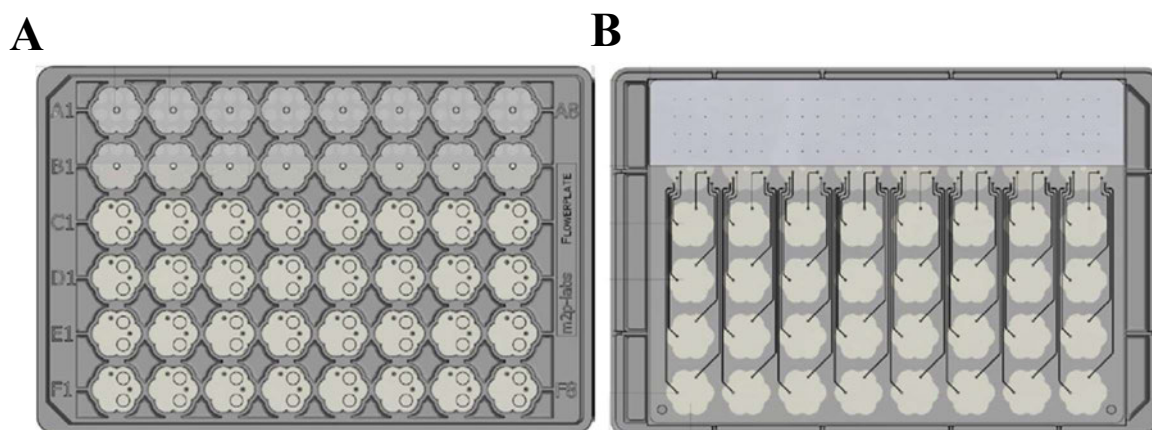
Figure 5: Schematic representation of the microfluidic FlowerPlate®. (A) Top view of the plate. The first two rows are reservoirs for the respective column below. (B) Bottom view of the plate. The membrane valves and the microchannels can be seen. (Source: https://www.m2p-labs.com, last visited: 06.04.2023)

Equally to the regular FlowerPlate®, the MF FlowerPlate® holds the same optodes. Hence, the addition of reservoir fluid can be triggered by using pH, DO, biomass or cultivation time set points.

Possible applications for the multifermenter system include strain screening, bioprocess development and optimization. For this thesis, it is particularly useful for testing different process conditions.

The BioLector® system is compatible with other laboratory automation systems like the Freedom EVO® 200 platform from TECAN, allowing for seamless integration into existing workflows.

2.7. Freedom EVO® 200 platform

The Freedom EVO® 200 platform from TECAN is an advanced robotic system designed for laboratory automation, including automated liquid handling and sample preparation. The platform is highly customizable, allowing researchers to tailor the system to their specific needs and workflows.

The platform used in this work was equipped with a liquid handling (LiHa) arm for pipetting, a robotic manipulator (RoMa) arm to move labware such as microtiter plates (MTP), a centrifuge, and a plate reader. The LiHa arm holds eight steel needles that can

be operated to aspirate or dispense liquids from microtiter plates and throughs located on different carriers on the deck. Each needle of the LiHa can pipette volumes between 10 and 980 µL. Thus, the LiHa can be used, for example, to pipette assays, harvest supernatants, or dilute samples.

The RoMa transports microtiter plates between different carriers on the deck, including the centrifuge and the plate reader. A picture of the platform setup with BioLector® integration can be seen in Figure 6.
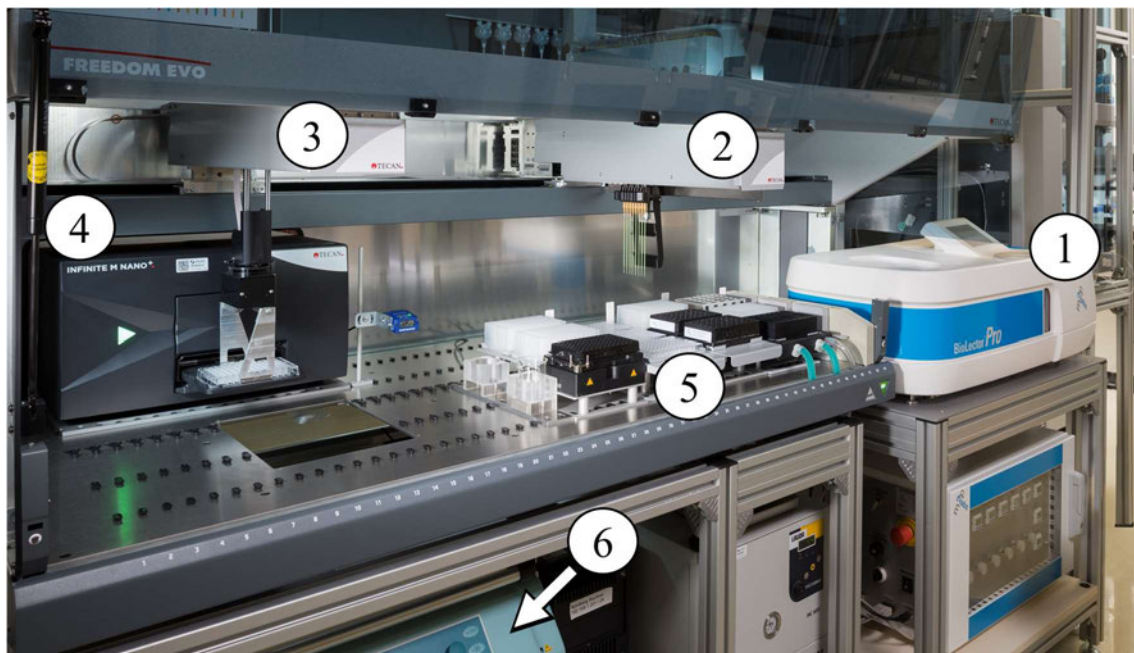
Figure 6: Picture of the automation platform for the workflow development. The platform contains a BioLector® multifermenter system (1), a LiHa for pipetting (2), a RoMa to transfer plates (3) a plate reader (4), a plate carrier for microtiter-, deep well- and BioLector® plates (5) as well as a centrifuge(6).

The Freedom EVO® 200 platform is controlled by the software called Freedom EVOware® by TECAN. The software is used to create workflow protocols controlling the respective instruments. Various parameters, such as pipetting volumes of the LiHa or plate layouts can be defined. This also includes instrument settings like centrifugation time and speed or the wavelength of the plate reader measurements.

2.8. Experimental approach

In the overlying EnzyPol project, one focus is to find optimal cultivation conditions to produce fungal peroxygenases in *K. phaffii* with regard to enzymatic activity, productivity and product yield. To achieve this goal, an automated and robust workflow is required. The workflow that was developed in this thesis contains a parallel micro-scale cultivation, protein quantification and enzyme activity assay. The cultivations of the POX-producing *K. phaffii* strain were conducted in the BioLector® Pro from Beckman Coulter GmbH. Here, different methanol induction profiles and methods were applied to identify the optimal conditions for inducing POX expression. Additionally, a Bradford protein assay was performed to determine the total protein concentration. Lastly, an ABTS assay was conducted to measure the enzyme activity for the respective cultivation conditions. Both assays were executed on the Freedom EVO® 200 platform from TECAN.

To automate the readout for POX activity, the ABTS assay was initially tested with various pipetting patterns on the Freedom EVO® 200 platform, with the goal of minimizing deviation within replicates. The automation also involved sample preparation, including centrifugation, supernatant harvesting, and sample dilution. Samples were obtained by cultivating *K. phaffii* in shake flasks, where POX production was induced using methanol. The Bradford assay for protein quantification was also automated using the TECAN platform. With accomplished automation of both the ABTS and Bradford assays, the next step is cultivation of *K. phaffii* using the BioLector® system. To achieve high cell densities and good reproducibility, the optimal concentrations of glycerol and glucose were evaluated. Furthermore, various methanol induction strategies such as (repetitive) pulses and continuous feeding were studied using the MF FlowerPlates®.

A scheme of the final workflow can be seen in Figure 7.
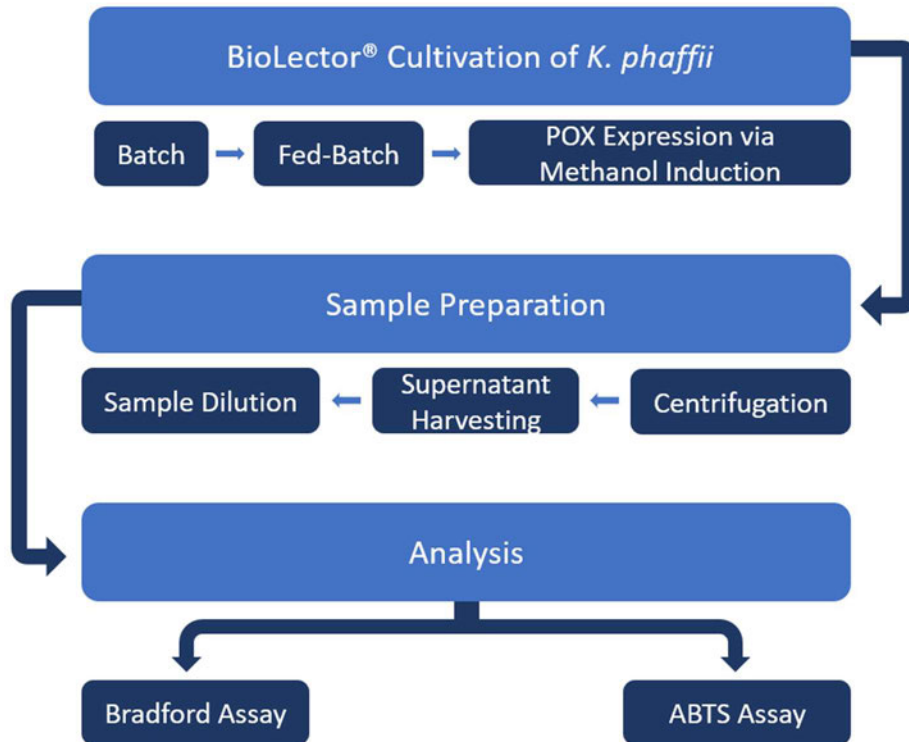
Figure 7: Schematic representation of the final automated, microcultivation and analytical workflow.

3. Materials

All devices, consumables and software used in this work can be seen in Table 1, Table 2 and Table 3, respectively. The media and their components are displayed from Table 4 to Table 16.

3.1. Devices

Table 1: List of devices

Device	Manufacturer
Autoclave FOB5/T2, FVA3/A1	Fedegari, Albuzzano, Italy
BioLector® Pro	Beckman Coulter, Brea, CA, USA
Cleanbench, 1540-V-10	Heraeus, Hanau, Germany
Freedom EVO® 200	Tecan Group Ltd., Männedorf, Switzerland
Freezer (-20 °C)	Siemens, München, Germany
Freezer (-80 °C)	Thermo Fisher Scientific, Waltham, USA
Fridge (4 °C), K3130	Liebherr, Bulle, Switzerland
Incubator Multitron Pro	Infors, Einsbach, Germany
MilliQ®-System, Omnia Pure System	stakpure GmbH, Niederahr, Germany
pH Electrode, S20 seven easy	Mettler-Toledo International Inc., Columbus, OH, USA
Photometer, UV1800	Shimadzu, Reinach, Switzerland
Pipettes, research plus	Eppendorf AG, Hamburg, Germany
Plate reader Infinite M Nano+	Tecan Group Ltd., Männedorf, Switzerland
Rotanta 460 robotic centrifuge	Hettich GmbH, Tuttlingen, Germany

3.2. Consumables

Table 2: List of consumables

Consumable	Manufacturer
96-well microtiter plate, f-bottom, black	Greiner BIO-ONE, Frickenhausen, Germany
Cryovials	Eppendorf AG, Hamburg, Germany
Cuvettes	Ratiolab, Dreieich, Germany

Consumable	Manufacturer
Deep Well Plates (1 mL)	Ritter Medical, Schwabmünchen, Germany
Flower Plate®, MTP-48-BOH1	m2p-labs, Baesweiler, Germany
Flower Plate®, MTP-MF32C-BOH 1	m2p-labs, Baesweiler, Germany
Micro reaction tubes 1.5 mL, 2 mL, 5 mL	Eppendorf AG, Hamburg, Germany
Coomassie (Bradford) Protein Assay Kit (Cat. No. 23200)	Thermo Fisher Scientific, Waltham, USA
Pipette tips 100-1000 µL	Eppendorf AG, Hamburg, Germany
Pipette tips 2-200 µL	Eppendorf AG, Hamburg, Germany
Reactiontube (15 mL, 50 mL)	TPP Techno Plastic Products AG, Trasadingen, Switzerland
Sealing Foil for Automation	m2p-labs, Baesweiler, Germany
Serological Pipettes	VWR International GmbH, Langenfeld, Germany
Silverseal sealer, aluminium foil	Greiner Bio-One, Frickenhausen, Germany
Sterile filter, Nalgene® 0.2 µM	Thermo Fisher Scientific, Waltham, USA

3.3. Software

Table 3: List of software

Software	Manufacturer
BioLection	Beckman Coulter, Brea, CA, USA
Freedom EVOware®	Tecan Group Ltd., Männedorf, Switzerland
GraphPad Prism 9	GraphPad Software, Inc., Boston, MA, USA
Python	Python Software Foundation, DE, USA
Visual Studio Code	Microsoft Corporation, Redmond, WA USA

3.4. Media

All used media and their respective compositions are shown in Table 4 to Table 16.

Table 4: YPG Medium composition

Component	Stock concentration [g/L]	Final concentration [g/L]	Volume [mL]
YP Base	60	30	500
Glycerol	500	20	40
Zeocin	100	0.15	2.5
Add MilliQ to Final Volume of:			1000

Table 5: YP Base composition

Component	Mass [g]
Yeast Extract	20
Peptone	40
Add MilliQ to Final Volume of:	1000 mL

Table 6: BMD1 Media composition

Component	Stock concentration [g/L]	Final concentration [g/L]	Volume [mL]
Potassium Phosphate Buffer B			200
Yeast Nitrogen Base	134	13,4	100
Glucose	200	10	50
Biotin	0,2	0,0004	2.0
Zeocin	100	0.15	2.5
Add MilliQ to Final Volume of:			1000

Table 7: BMM10 Medium composition

Component	Stock concentration [g/L]	Final concentration [g/L]	Volume [mL]
Potassium Phosphate Buffer B			200
Yeast Nitrogen Base	134	13.4	100
Methanol	790	39.5	50
Biotin	0.2	0.0004	2.0
Zeocin	100	0.15	2.5
Add MilliQ to Final Volume of:			1000

Table 8: Potassium Phosphate Buffer A composition

Component	Sum Formula	Mass [g]
Potassium phosphate dibasic	K_2HPO_4	0.82
Add MilliQ to Final Volume of:		1000 mL

Table 9: Potassium Buffer B composition

Component	Sum Formula	Mass [g]
Potassium phosphate monobasic	KH_2PO_4	0.82
Adjust to pH 6 with Potassium Phosphate Buffer A		
Add MilliQ to Final Volume of:		1000 mL

Table 10: BSM Medium composition

Component	Sum Formula	Mass [g]
Citric acid	$C_6H_8O_7$	1.96
Calciumchlorid dihydrat	$CaCl_2 \cdot 2\ H_2O$	0.02
Ammonium sulfate	$(NH_4)_2SO_4$	12.6
Magnesium sulfate heptahydrate	$MgSO_4 \cdot 7\ H_2O$	0.5
Potassium chloride	KCl	0.9
Potassium phosphate monobasic	KH_2PO_4	1.0
Potassium phosphate dibasic	K_2HPO_4	1.0
Biotin		2.0 mL
PTM1 Trace Salts		4.6 mL
Glycerol or Glucose		Depending on desired concentration
Add MilliQ to Final Volume of:		1000 mL

Table 11: PTM1 Trace Salts composition

Component	Sum Formula	Mass [g]
Boric acid	H_3BO_3	0.02
Cobalt(II) chloride hexahydrate	$CoCl_2 \cdot 6\ H_2O$	0.82
Sodium iodide	NaI	0.08
Sodium molybdate dihydrate	$Na_2MoO_4 \cdot 2\ H_2O$	0.2
Copper(II) sulfate pentahydrate	$CuSO_4 \cdot 5\ H_2O$	6.0
Iron(II) sulfate heptahydrate	$FeSO_4 \cdot 7\ H_2O$	0.025
Manganese(II) sulfate monohydrate	$MnSO_4 \cdot H_2O$	3.36
Zinc chloride	$ZnCL_2$	20
Sulfuric acid	H_2SO_4	2.717
Add MilliQ to Final Volume of:		1000 mL

Table 12: BSM Feed Medium composition

Component	Sum Formula	Mass [g]
Calciumchlorid dihydrat	$CaCl_2 \cdot 2\ H_2O$	0.35
Magnesium sulfate heptahydrate	$MgSO_4 \cdot 7\ H_2O$	6.45
Potassium chloride	KCL	10
Glycerol		400
Biotin		6.0 mL
PTM1 Trace Salts		15 mL
Add MilliQ to Final Volume of:		1000 mL

Table 13: ABTS Assay Solution composition

Component	Stock concentration [mol/L]	Final concentration [mol/L]	Volume [mL]
ABTS Stock	0.02	0.001	1
H_2O_2 Solution (3 %)	1.29	0.0005	0.00775
Sodium Citrate Solution	0.21	0.2	19

Table 14: ABTS Stock composition

Component	Sum Formula	Mass [g]
ABTS		0.55
Sodium acetate	$C_2H_3NaO_2$	0.34
Add MilliQ to Final Volume of:		1000 mL

Table 15: Hydrogen Peroxide Solution composition

Component	Volume [mL]
Hydrogen Peroxide (30%)	100
Add MilliQ to Final Volume of:	1000

Table 16:Sodium Citrate Solution composition

Component	Sum Formula	Mass [g]
Trisodium citrate	$Na_3C_6H_5O_7$	61.96
Add MilliQ to Final Volume of:		1000 mL

3.5. Cell lines

Two strains of the *K. phaffii* organism were used in this work. The wild type (WT) and a genetically modified strain *K. phaffii* BSYBG11JP-HP_pBSY5S1Z_POX12_G1. In the following, the strains will be referred to as WT and POX12, respectively. The exact modifications of the POX12 strain were not elaborated, however, the strain inherits a PDF promotor in its expression cassette. The POX12 strain was provided by the bisy GmbH (a project partner of the EnzyPol project) and the WT by the Forschungszetrum Jülich.

4. Methods

4.1. Cultivation of *K. phaffii*

This chapter covers all methods concerning the cultivation of *K. phaffii* in different scales and systems, as well as POX production and methanol addition. All these operations were conducted in a sterile environment working in a class II biological safety cabinet. The working space as well as all devices were cleaned with Bacillol® before and after use.

4.1.1. Strain maintenance

The optical density$_{600}$ (OD$_{600}$) from a pre-culture cultivation (chapter 4.1.2.1) was measured and the cells were centrifuged at 4000 rpm (2898 g) and 4 °C for 10 min. The cell pellet was then resuspended in fresh YPG media to an OD$_{600}$ of 90. Then 500 µL cell suspension was mixed with 500 µL of 50 % (v/v) glycerol and stored in cryovials at - 80 °C.

4.1.2. Shake flask cultivations

4.1.2.1. Pre-culture cultivation

A cryogenic culture of the *K. phaffii* strain of choice was used to inoculate 50 mL YPG medium in an unbaffled, 500 mL Erlenmeyer flask. Note that Zeocin was not added to the YPG media when the WT strain was cultivated. The yeast was cultivated at 250 rpm and 30 °C for 24-36 h.

4.1.2.2. Main-cultivation and POX expression for ABTS and Bradford assay

An unbaffled Erlenmeyer flask was prepared with 50 mL BMD1 medium and inoculated with a starting OD$_{600nm}$ of 0.1 from a pre-culture (see chapter 4.1). The cells were cultivated at 250 rpm and 30 °C for 60 h. To induce POX expression, 5.55 mL of BMM10 medium was added to the shake flask culture and cultivated for 8 h under the same conditions as before. After that, 0.55 mL BMM10 medium was added to the culture in three consecutive inductions, each spaced 24 h apart. Then, the culture was centrifuged at 4000 rpm (2898 g) and 4 °C for 20 min. Finally, the supernatant was aliquoted and either analyzed immediately or frozen at -20 °C for later use.

4.1.3.   Cultivation of *K. phaffii* in the BioLector®
4.1.3.1. Batch cultivation

A respective amount of BSM medium was inoculated with OD_{600nm} of 0.3 from a pre-culture (see chapter 4.1.2.1). Note, that BSM media with different C-sources and concentrations were used. Hence, 1 mL of inoculated BSM medium was pipetted into the respective wells of a FlowerPlate®. The plate was then covered with a sealing film and placed in the BioLector®.

The cultivation parameter included the time between measurements with 13 min, a shaking frequency of 1000 rpm, a humidity control of 85 % and the cultivation temperature of 30 °C. The humidity and temperature were measured in the cultivation chamber. The cells were cultivated for a total of 72 h.

After the cultivation, the plate was placed onto the dedicated plate carrier of the Freedom EVO® 200 platform for assay execution.

4.1.3.2. Fed-Batch cultivation

Similar to the batch cultivation, a respective amount of BSM medium was inoculated with OD_{600nm} of 0.3 from a pre-culture (see chapter 4.1.2.1). Note, that BSM media with different C-sources and concentrations were used. Afterwards, 800 µL inoculated medium was transferred into the respective wells in row C - F of a MF FlowerPlate®. Then, the reservoir wells in row A were filled with 1 mL of BSM feed-media, and row B with 1 mL of methanol solutions in respective concentrations. After covering the plate with a sealing film, the plate was put into the BioLector®.

The cultivation parameters remained the same as for batch cultivation (see chapter 4.1.3.1). The start and stop of the reservoir feeds were triggered using time setpoints. The fed-batch started after 26 h of cultivation and stopped after 42 h. Thereafter a 4 h waiting phase was implemented to allow the total consumption of glycerol from the BSM feed medium. Then, the methanol feed started after 46 h of cultivation and continued for 48 h. Hence, the total cultivation time was 94 h. The cultivation timeline can be seen in Figure

8. Both feeding profiles were linear. The feeding rate of the BSM feeding medium was set to 10 µL/h, thus, a total of 160 µL was fed in 16 h into each well. The methanol feed was 3.5 µL/h for a total fed volume of 168 µL.
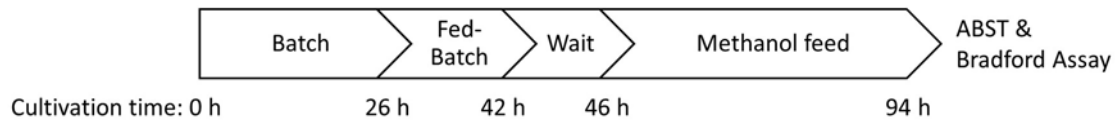
Figure 8: Timeline of the fed-batch cultivation of *K. phaffii* with methanol feed.

After cultivation, the plate was placed onto the dedicated plate carrier of the Freedom EVO® 200 platform for automated analytical procedures.

4.1.4. POX expression of *K. phaffii* during BioLector cultivation®

4.1.4.1. Methanol induction via manual pipetting

The manual methanol pulses were carried out during batch cultivation of *K. phaffii* in the BioLector® (see chapter 4.1.3.1).

First, methanol was diluted to the respective concentration using $H_2O_{dist.}$. The methanol solution was pipetted into the dedicated well of the FlowerPlate® by piercing the gas permeable membrane through the self-resealing slit of the plate sealing film. A total of seven pulses with 20 µL each were performed. The pulse time points were 45 h, 47 h, 49 h, 51 h and 53 h as well as 69 h and 71 h.

4.1.4.2. Methanol induction via microfluidic

The POX production and methanol feed via MF was carried out during a fed-batch cultivation of *K. phaffii* in the BioLector® (see chapter 4.1.3.2).

After 46 hours of fed-batch cultivation, the methanol feeding started. With the MF, 3.5 µL of the respected methanol feed was added to the cultivation wells for 48 hours, for a total volume of 168 µL methanol fed in each cultivation well.

4.2. Analytic of enzyme activity and protein quantification
4.2.1. Bradford assay

The Bradford assay was first conducted manually to assess the rough protein concentration that can be expected after *K. phaffii* cultivation and to gain insights for the successive automation of the assay.

4.2.1.1. Manual Bradford assay execution

The Bradford assay was executed as explained in the Standard Test Tube Protocol of the Coomassie (Bradford) Protein Assay Kit (Cat. No. 23200) instruction manual.

First, the Albumin (BSA) standards were prepared, as shown in Table 17.

Table 17: Dilution scheme of BSA standards for manual Bradford assay

Vial	$V_{Diluent}$ [µL]	$V_{BSA\ Source}$ [µL]	C_{BSA_Final} [µg/mL]
A	0	300 (Stock)	2000
B	125	375 (Stock)	1500
C	325	325 (Stock)	1000
D	175	175 (Vial B)	750
E	325	325 (Vial C)	500
F	325	325 (Vial E)	250
G	325	325 (Vial F)	125
H	400	100 (Vial G)	25
I	400	0	0

30 µL of each standard and sample was pipetted into a 2 mL reaction tube. Standards were applied in duplicates and samples in triplicates. Then, 1.5 mL Coomassie reagent (equilibrated to room temperature (RT)) was added and the tubes were incubated for 10 minutes at RT. Subsequently, the solutions were decanted into cuvettes and measured spectrophotometrically at a wavelength of 595 nm.

To correct the data, the average measurement of the blank replicates was subtracted from all other measurements. Then, a standard curve was created, by plotting the average

measurements from the BSA standards against their respective concentrations. The protein concentrations of the unknown samples were then interpolated using Equation 1.

Equation 1: Calculation of protein concentration using the Bradford assay.

$$c_{unkown\ sample} = \frac{Absorption_{unkown\ sample} - b_{Standard\ curve}}{m_{Standard\ curve}} \quad (1)$$

with:

m = slope

b = y-axis interception

4.2.1.2. Automation of the Braford assay on the TECAN Freedom EVO® 200 platform

For the automated Bradford assays, the BSA standards were prepared as shown in Table 18.

Table 18: Dilution scheme of BSA standards for automated Bradford assay

Vial	$V_{Diluent}$ [µL]	$V_{BSA\ Source}$ [µL]	C_{BSA_Final} [µg/mL]
A	125	375 (Stock)	1500
B	400	400 (Stock)	1000
C	192.5	157.5 (Stock)	900
D	210	140 (Stock)	800
E	175	175 (Vial A)	750
F	400	400 (Vial B)	500
G	271.25	78.75 (Stock)	450
H	280	70 (Stock)	400
I	288.75	61.25 (Stock)	350
J	297.5	52.5 (Stock)	300
K	325	325 (Vial F)	250
L	210	140 (Vial F)	200
M	245	105 (Vial F)	150
N	325	325 (Vial K)	125
O	400	100 (Vial N)	25
P	400	0	0

In a first step, 800 µL of cell culture was harvested from the 48-Well FlowerPlate®, or 32-Well microfluidic FlowerPlate®, respectively, and pipetted into a 1 mL, 96-well, deep-well plate (DWP). A tara plate was then pipetted by transferring 800 µL of water into another 1 mL, 96-well, DWP. Next, both plates were transferred into the centrifuge and centrifuged for 10 minutes at 4000 rpm (2898 g). Thereafter, the plates were transferred back and 700 µL of supernatant was pipetted into a new 1 mL 96-well, deep well plate.

To prepare the samples for the assay, 200 µL, 40 µL, and 20 µL of the supernatant was transferred to a new 1 mL DWPs. Dilution of the samples was achieved by adding 0 µL, 160 µL, or 180 µL of distilled water, respectively, resulting in undiluted, 1:5, and 1:10 diluted samples. Subsequently, 20 µL of these dilutions were transferred to new DWPs along with 20 µL of BSA standards, which were pipetted into separate wells of the DWP. The standards and samples were then mixed with 500 µL of Coomassie solution, and 200 µL of the resulting solution was transferred to a MTP for absorbance measurement at 595 nm using a plate reader.

4.2.2.   ABTS assay

The ABTS assay was once conducted manually to assess the rough enzymatic activity that can be expected after *K. phaffii* cultivation and to gain insights for the successive automation of the assay. Hence, the assay pipetting was automated, and the workflow was successively optimized.

4.2.2.1. Manual ABTS assay execution

To calculate the volumetric POX activity, Equation 2 is used.

Equation 2: Calculation of enzymatic activity.

$$U = \frac{\left(\frac{\Delta A}{\Delta t}*V_{tot}*D\right)}{V_{sample}*\varepsilon*d*R} \tag{2}$$

with the variables:

$\frac{\Delta A}{\Delta t} :=$ Change in absorption per time [min^{-1}]

$D :=$ Dilution factor for the sample [-]

$U :=$ Units per mL [µmol · mL^{-1} · min^{-1}]

and the constants:

$V_{tot} :=$ Total assay volume [mL] = 0.2

$V_{sample} :=$ Sample volume [mL] = 0.02

$d :=$ Layer thickness [cm] = 1

$R :=$ Correlation coefficient between photometer and plate reader [-] = 0.998

$\varepsilon :=$ Extinction coefficient at 405 nm [mL $\cdot$ μmol^{-1} $\cdot$ cm^{-1}] = 36

4.2.2.2. Automation of the ABTS assay on the TECAN Freedom EVO® 200 platform

Since optimizing the ABTS assay workflow was one of the key aspects of this thesis, multiple versions were developed and will be elaborated as relevant. However, the following process was employed for all versions. All steps in this process were carried out automatically with the help of the robotic system (*e.g.*, LiHa for pipetting and RoMa for transferring labware).

The supernatant for the ABTS assay was obtained as explained in 4.2.1.2.

To dilute the supernatant, 200 µL of supernatant was pipetted into another 1 mL DWP and followed by adding 800 µL of ABTS assay buffer for a 1:5 dilution. Subsequently, 20 µL of the diluted samples were pipetted into a clear 96-well flat-bottomed Greiner plate. Lastly, 180 µL of ABTS assay solution was added to each sample, and the plate was placed in the plate reader to measure the kinetic absorption at 405 nm every 15 s. Total measurement time was first set to 120 min and later reduced to 30 min (see respective experiment).

4.3. Data evaluation

The ABTS assay and cultivation data was evaluated using the computational environment Jupyter Notebook, with Python as the programming language. Data evaluation included loading the raw data, filtering, and visualization. For visualization, the mean value of replicates is shown as a solid line, and the standard deviation is shown as an aerial range.

The ABTS assay analysis also included the calculation of the minimal, maximal, and average enzymatic activity as well as the average of the percentage deviations between replicates. For evaluation of the Bradford assay, the program GraphPad Prism 8 was used.

5. Results
5.1. Establishment and automation of ABTS assay

The overall goal of the ABTS assay experiments was to evaluate the respective assay workflow on the Freedom EVO® platform in terms of accuracy and precision. The assay workflows were then adapted by, *e.g.*, changing the pipetting volumes or layouts, and the results were analysed to assess the feasibility.

To begin with, the ABTS assay was pipetted manually to obtain data for comparison with the succeeding automated assay. The samples were obtained at the end of a shake flask cultivation with POX production and methanol induced MUT pathway (see chapter 4.1.2.2). The samples were diluted 1:5 and 1:50 prior conducting the ABTS assay. 96 technical replicates were measured for each dilution. Results can be seen in Figure 9.
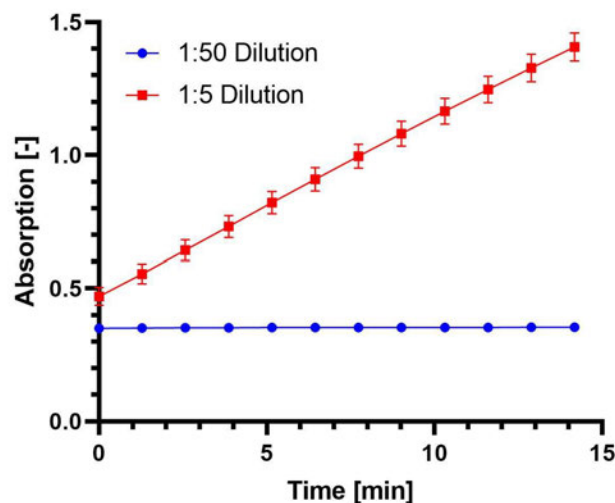
Figure 9: Manually conducted ABTS assay with different sample dilutions. Samples were diluted with ABTS assay buffer. 96 technical replicates were measured for each dilution.

As visible in Figure 9, the 1:5 diluted samples demonstrate a significant and observable increase in absorption over time. Hence, this dilution was consistently utilized for all subsequent ABTS assays in the study.

After the manually conducted assay, a workflow was created on the Freedom EVO® 200 platform for automated execution. This newly created workflow was initially tested to assess the first automated assay run for possible optimization. Here, samples from a shake flask cultivation with POX expression were used (see chapter 4.1.2.2). The samples were manually pipetted into a FlowerPlate® for direct connection to future microcultivation. Since the assay plate was a 96-well microtiter plate, the layout of the 48-well Flower-Plate® is pipetted twice into the assay plate. 42 technical replicates of the cell suspension and six negative controls (no cells, just ABTS buffer and assay solution) were pipetted in the FlowerPlate®. The general layout and pipetting steps can be seen in Figure 10 and the results of the assay are displayed in Figure 11.
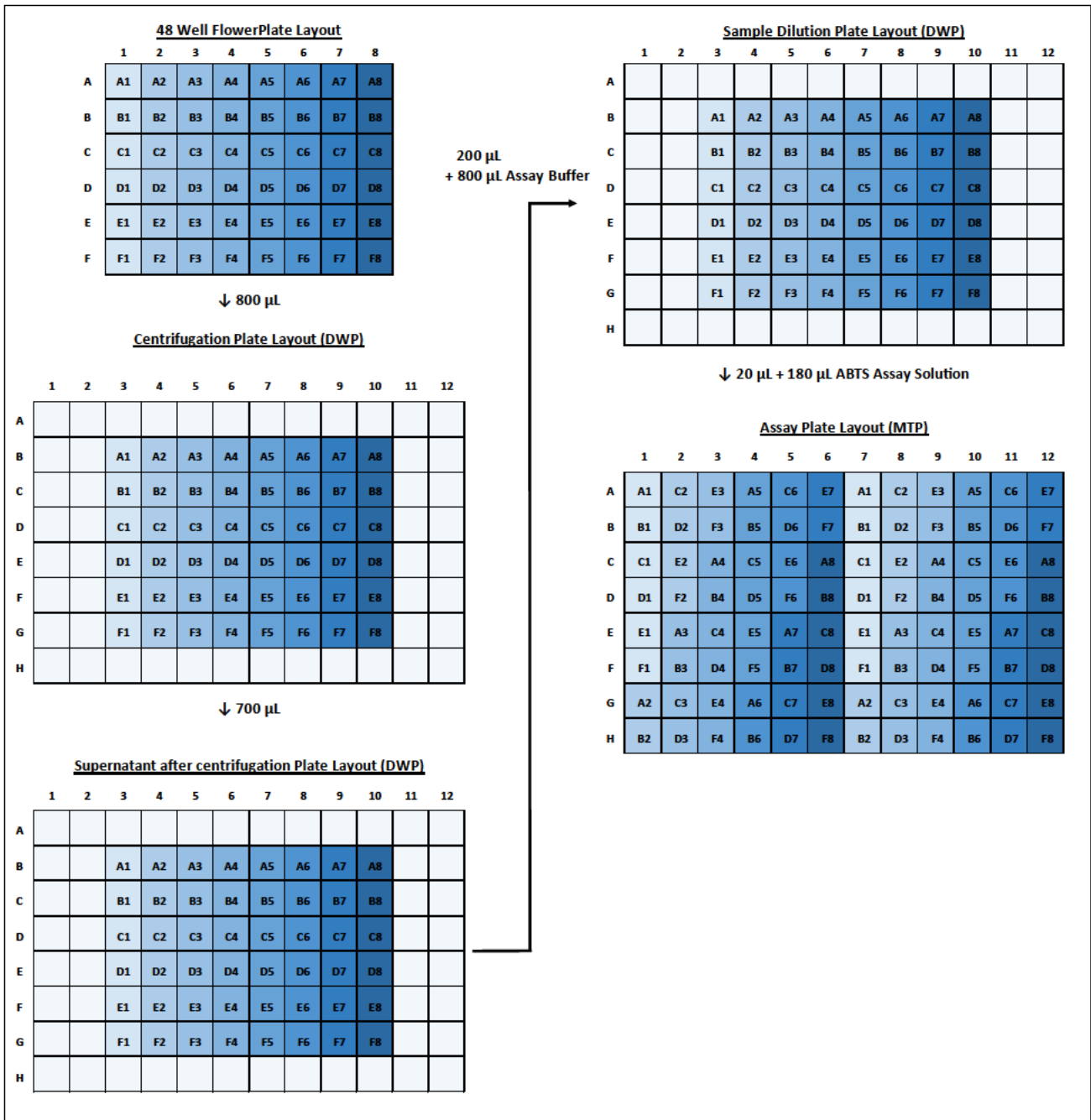
Figure 10: Schematic representation of the pipetting layout of the first conducted ABTS assay. The figure shows the initial layout of the 48-well FlowerPlate® and how it is transferred into the DWP and MTP, respectively. In addition, the pipetted volumes are shown. Each column of the layout has a different colour to better follow the pipetting scheme.

Two graphs can be seen in Figure 11 representing the mean values of the samples and the negative control.
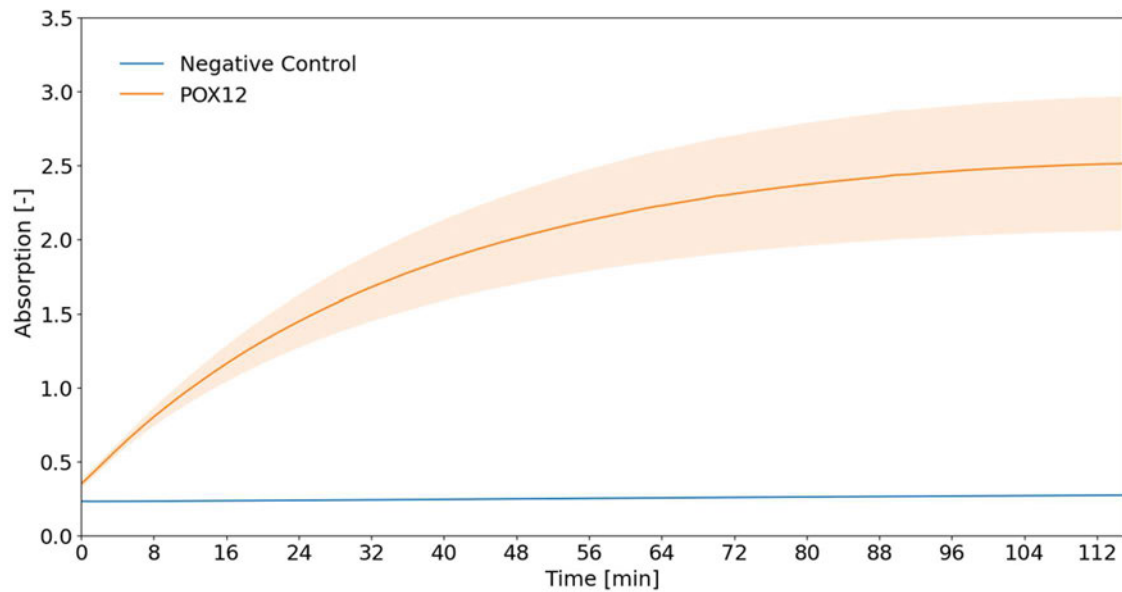
Figure 11: Evaluation of the first conducted ABTS assay workflow on the automation platform. The *K. phaffii* POX12 strain as well as the negative control can be seen. The POX12 samples were measured as 42 technical replicates, the negative control as 6 technical replicates.

Because the deviation between the replicates was considered unusually high, the data was plotted as a heatmap to evaluated possible plate effects. Here, the last measured absorbance of each well is shown. Considering the results, the data was plotted again taking the observed 'left-right' plate effect into account by plotting the replicates of the left and right plate sides as independent graphs. This is shown in Figure 12.
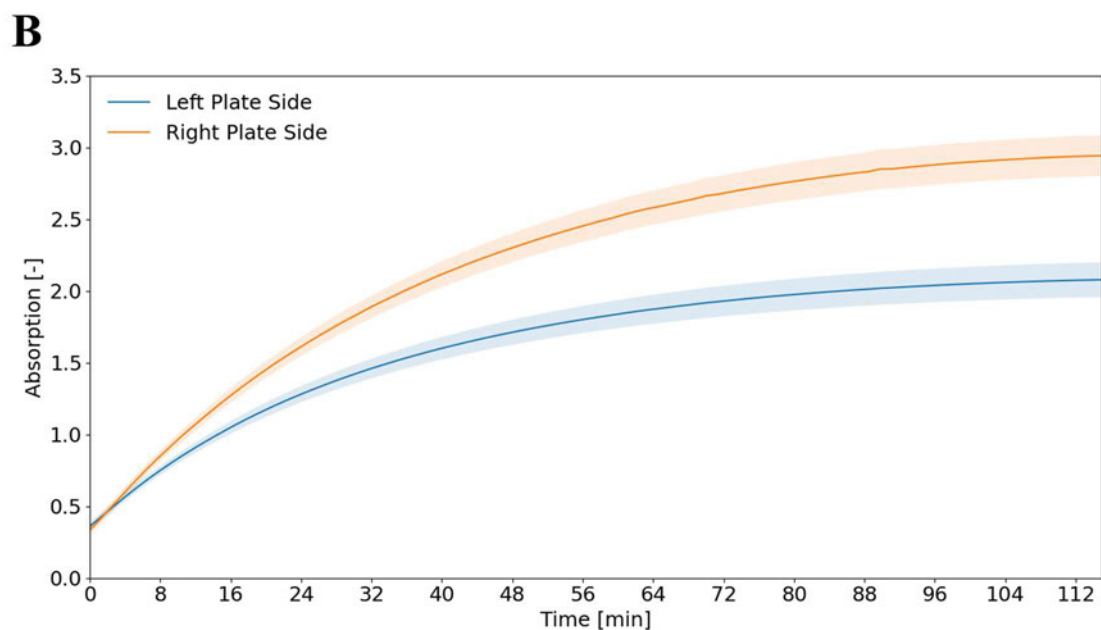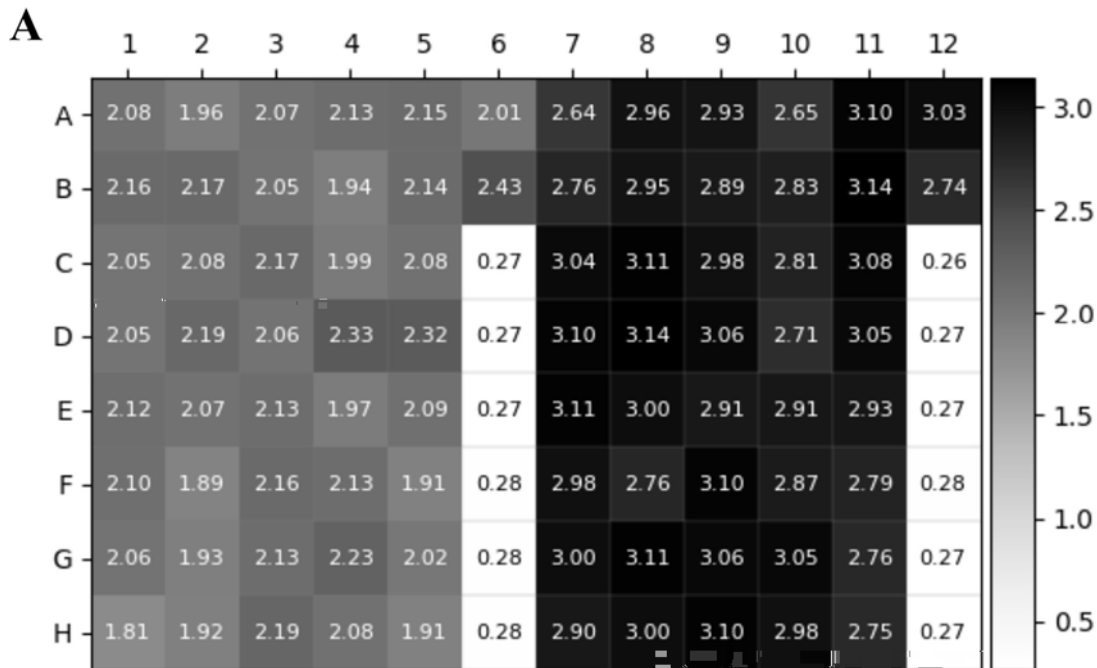
Figure 12: Visualization of the plate effect of the first automated ABTS assay. Each graph represents 22 technical replicates. (A) The absorption of each well is shown to observe a possible plate effect. The darker the well, the higher the absolute value of the absorption at the end of the measurement. (B) The replicates from the left and from the right side of the plate are plotted in separate graphs to better observe the observed plate effect.

For this first automated assay workflow several pipetting steps were done as multi-dispense steps. Here, a solution is aspirated and then dispensed several times, *e.g.*, when pipetting 20 μL from the sample dilution plate to the assay plate (see Figure 11). Hence,

40 µL of sample solution was aspirated and then 20 µL were dispensed twice into the respective wells.

The next assay workflow was adapted to minimize multi-dispense steps where possible. In addition, more washing steps were added between sampling and pipetting. The same sample from the last experiment was used. A 96-well MTP was pipetted entirely with this sample, so 96 technical replicates were created. To determine the enzymatic activity, it was necessary to establish the timespan in which the absorption over time is linear. For this purpose, a linear regression analysis was performed, which was fitted to the maximum number of data points possible while maintaining a coefficient of determination (R-squared) greater than or equal to 0.99. The results showed that this criterion is satisfied within the first 8 minutes of measurement. Hence, this condition was used for all calculations of enzymatic activity. The result of the assay is displayed in Figure 13.

A

B
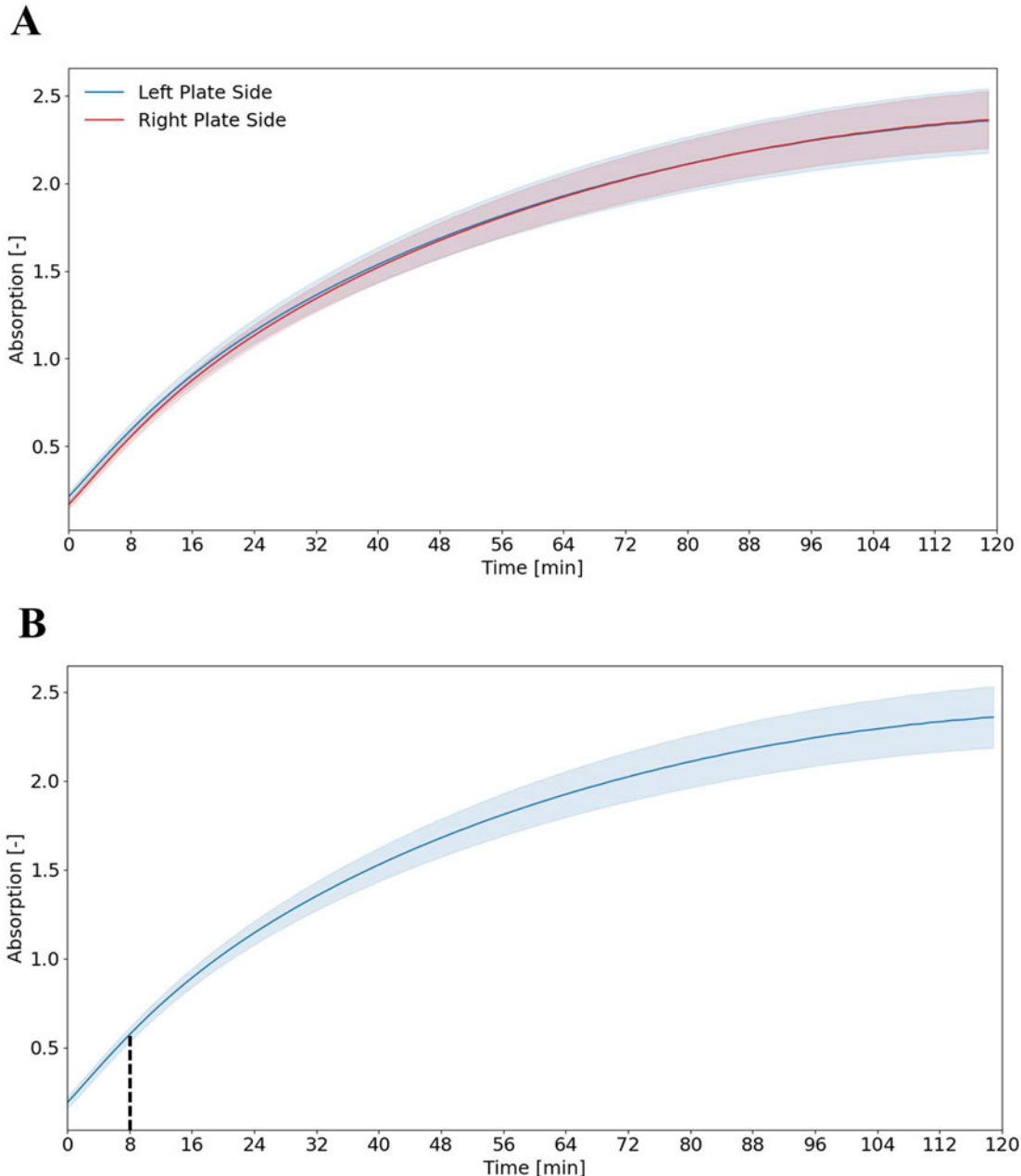
Figure 13: Result of the second ABTS assay workflow. A total of 44 technical replicates were tested. (A) The data was divided into the respective plate side to observe if the plate effect is still present. (B) The results of the whole plate, without separation into left and right plate side can be seen. At t = 8 min, a perpendicular line was drawn to indicate the endpoint of the time frame used for calculating the enzymatic activity.

In Figure 13 (A), one can see that there is no "left-right" position effect visible anymore. For this assay, the mean enzymatic activity U_{mean} and the average percentage deviation $U_{avg\%D}$ of the replicates within the first 8 min of the assay were calculated:

$U_{mean} = 0.065$ µmol/min and $U_{avg\%D} = 4.5$ %.

Thereafter another assay was performed with the purpose to test the sensitivity of the assay. Thus, the same sample as before was now diluted prior assay execution. Dilution factors were: undiluted, 1:2, 1:5 and 1:10 with ABTS assay buffer. Note, that all samples were again diluted 1:5 with ABTS assay buffer during the assay. To cut the overall assay time, the duration of the measurement was reduced to 30 minutes. The graphs of the assay measurements are shown in Figure 14, the calculated enzymatic activity can be seen in Table 19.
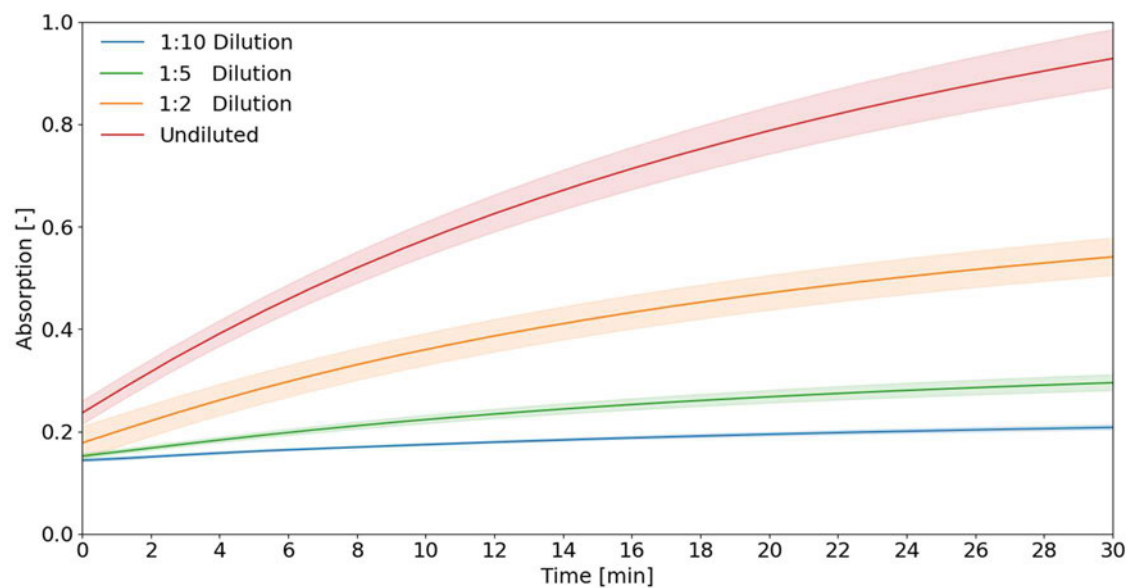
Figure 14: ABTS assay with different sample dilutions. The sample was diluted to analyse the sensitivity of the assay. Note that the dilution refers to the dilution pre-assay execution and all samples were still diluted 1:5 with ABTS assay buffer. For each condition, 12 technical replicates were tested.

Table 19: Mean enzymatic activity and average percentage deviation of the ABTS assay with different sample dilutions.

	Dilution Factor			
	Undiluted	1:2	1:5	1:10
$U_{mean} =$ [µmol/min]	0.049	0.053	0.051	0.046
$U_{avg\%D} =$	5.6 %	5.1 %	7.5 %	8.9 %

Figure 14 shows that for the starting absorption at $t = 0$ min, different diluted samples show different y-axis interceptions. Hence, for the next assay, modifications were made to the pipetting layout and measurement procedure. In order to minimize the interval between pipetting the ABTS assay solution into the sample and obtaining the absorbance reading, the assay plate was divided into three segments that were measured independently. In detail, after transferring 20 µL of sample solution into the assay plate, 180 µL of ABTS assay solution was added into the first of three segments only. This segment was then analysed first in the plate reader. Afterwards, assay solution was added to the second segment, and the absorption was measured once again. This process was then repeated for the last segment of the assay plate. The sample used in this assay was obtained from a 1 L fed-batch fermentation with methanol induced POX expression. The sample was provided by my supervisor Christian Wagner, who conducted the fermentation. A schematic depiction of the plate segments and the measured absorbance graphs are shown in Figure 15, in Table 20 the enzymatic activity can be seen.
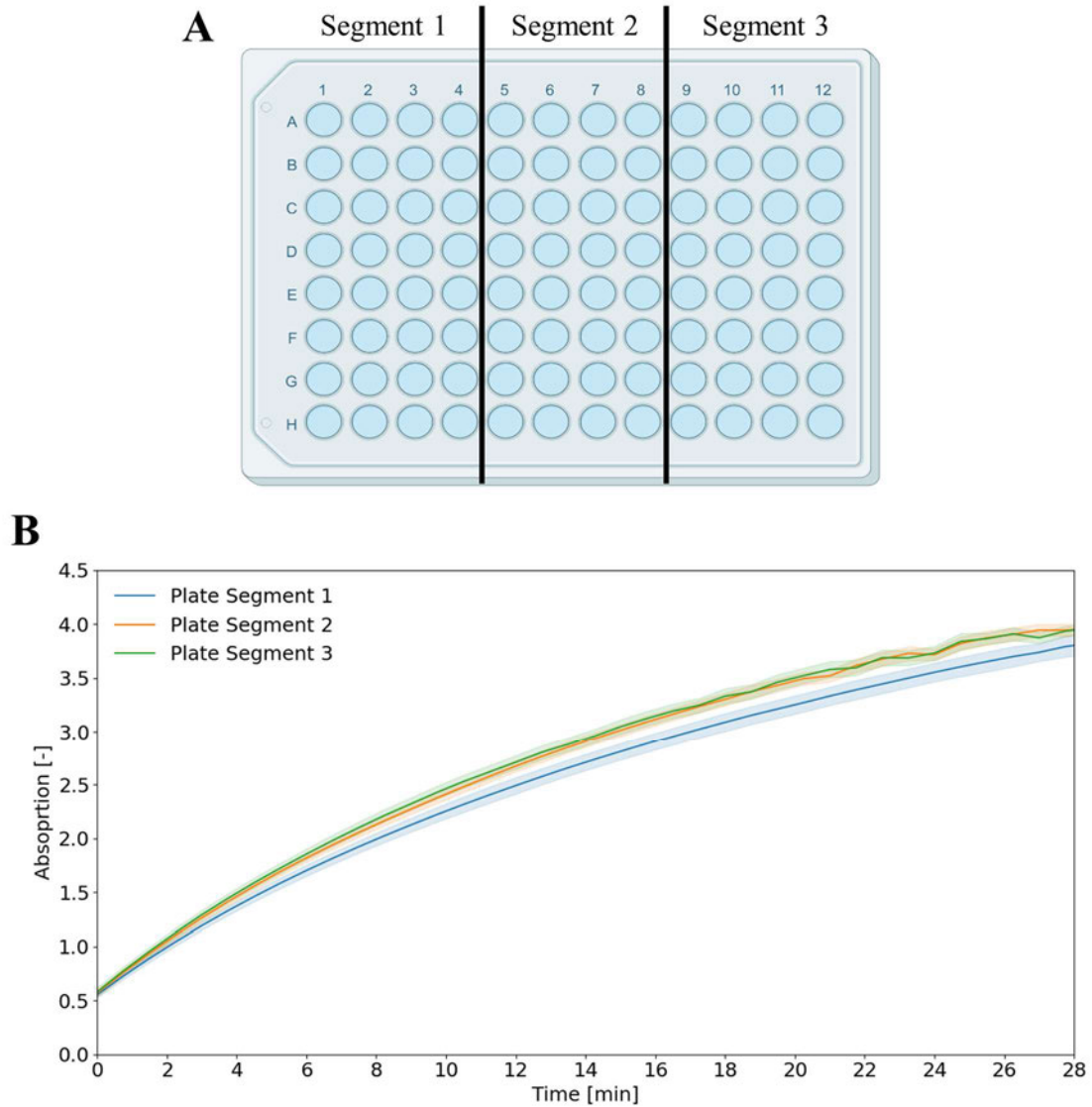
Figure 15: ABTS assay measurement of segmented assay plate. The measurement procedure of the assay plate was optimized to reduce the timespan between ABTS assay solution pipetting and measurement. 96 technical replicates were measured. (A) Schematic representation of the plate segment that were pipetted and measured independently. (B) Mean ABTS assay measurement of each segment.

Table 20: Mean enzymatic activity and average percentage deviation of the ABTS assay of different plate segments.

	Plate Segment		
	1	2	3
U_{mean} = [$\mu mol/min$]	0.26	0.28	0.28
$U_{avg\%D}$ =	1.9 %	1.2 %	1.8 %

As the deviation of U_{mean} and $U_{avg\%D}$ between segments were low (see Table 20), the robotic platform implementation of the assay was deemed successful. Consequently, all subsequent ABTS assays were conducted following the same procedure.

5.2. Establishment and automation of Bradford assay

To obtain data for comparison with the subsequent automated assay, a manual Bradford assay was initially performed using the same sample as in the last ABTS assay (Figure 15). The undiluted sample was measured, as well as 1:2, 1:5, and 1:10 dilutions. The standards were measured in technical duplicates, while the samples were measured in technical triplicates. In Table 21 the absorption measurements of the Bradford standards can be seen. Figure 16 show the corresponding linear regression of those standards and the interpolated protein concentration. Note that the accuracy of the calculated protein concentrations depends on the accuracy of the calibration curve. Thus, the linear regression of the standards was limited to 1000 µg/mL to obtain a coefficient of determination > 0.98.

Table 21: Bradford standard measurements of the manually pipetted assay.

Bradford Standards (manually pipetted assay)	
$c_{Protein}$ [µg/mL]	Δ Absorption [-]
0	0.512
25	0.529
125	0.681
250	0.829
500	1.133
750	1.376
1000	1.526
1500	1.733
2000	1.824

A
Bradford Assay Standards
(manually pipetted)

B
Bradford Assay Samples
(manually pipetted)
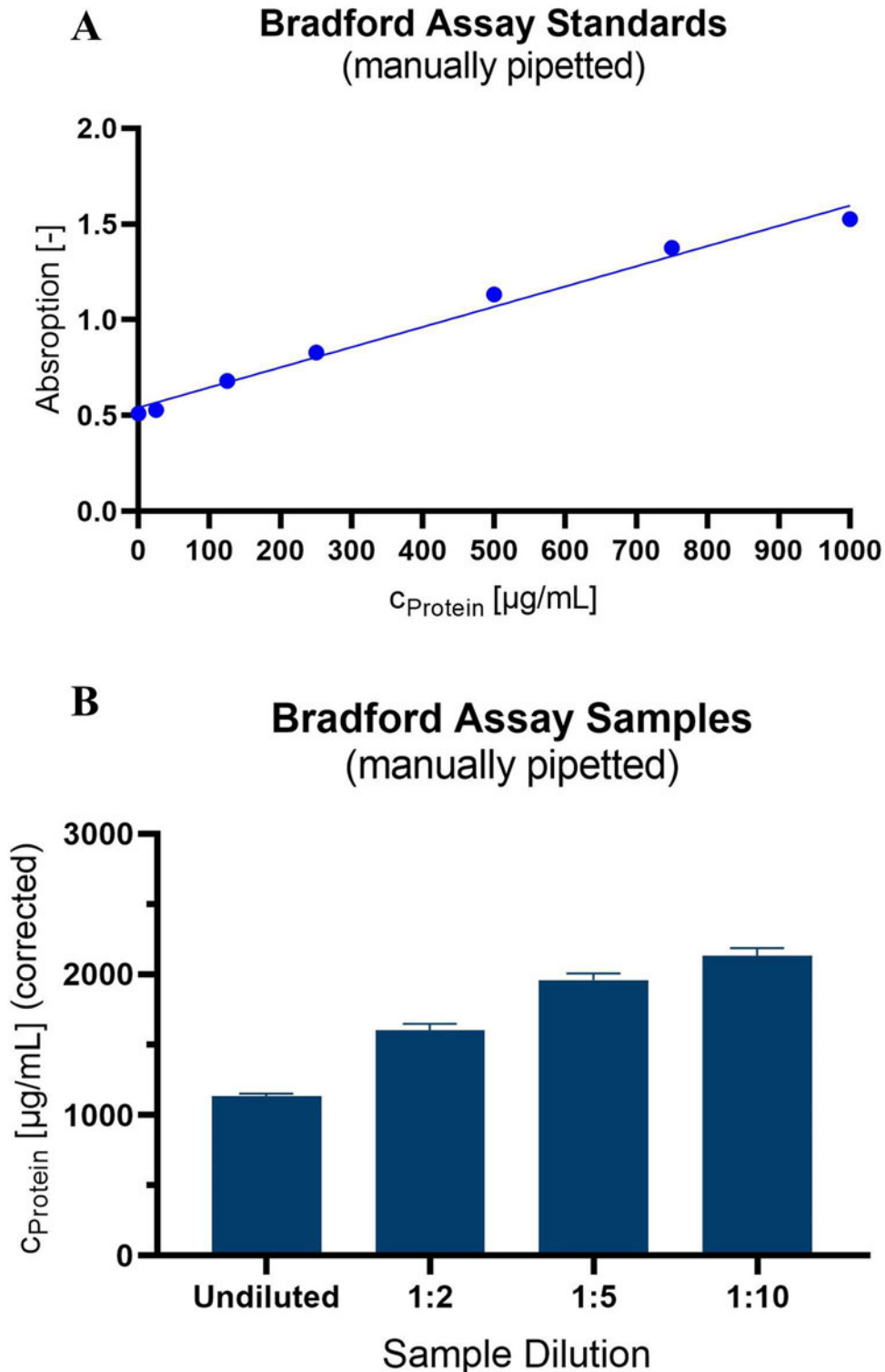
Figure 16: Bradford measurements of the manually pipetted assay. (A) Linear regression of the assay standards. The regression was only fitted until $1000 \, \mu g/mL$ to ensure a coefficient of determination > 0.98. (B) The corrected protein concentration of the diluted samples. The higher the dilution, the higher the corrected protein concentration.

As a next step, a workflow was created on the automation platform. Hence, the assay was performed with samples from a 1 L fed-batch fermentation with POX12. The samples were again provided by Christian Wagner who conducted the fermentation. The sample was measured undiluted, 1:5 and 1:10 diluted in technical quadruplicates. Standards were measured in technical duplicates. Table 22 shows the measured values of the BSA standards. In Figure 17, the linear regression of the standards and the calculated, corrected protein concentration of the sample can be seen.

Table 22: Bradford standard measurements of the automated assay.

Bradford Standards (automated assay)	
$c_{Protein}$ [µg/mL]	Δ Absorption [-]
0	0.430
25	0.491
125	0.576
150	0.612
200	0.670
250	0.668
300	0.825
350	0.877
400	0.797
450	0.846
750	1.146
800	1.159
900	1.180
1000	1.218
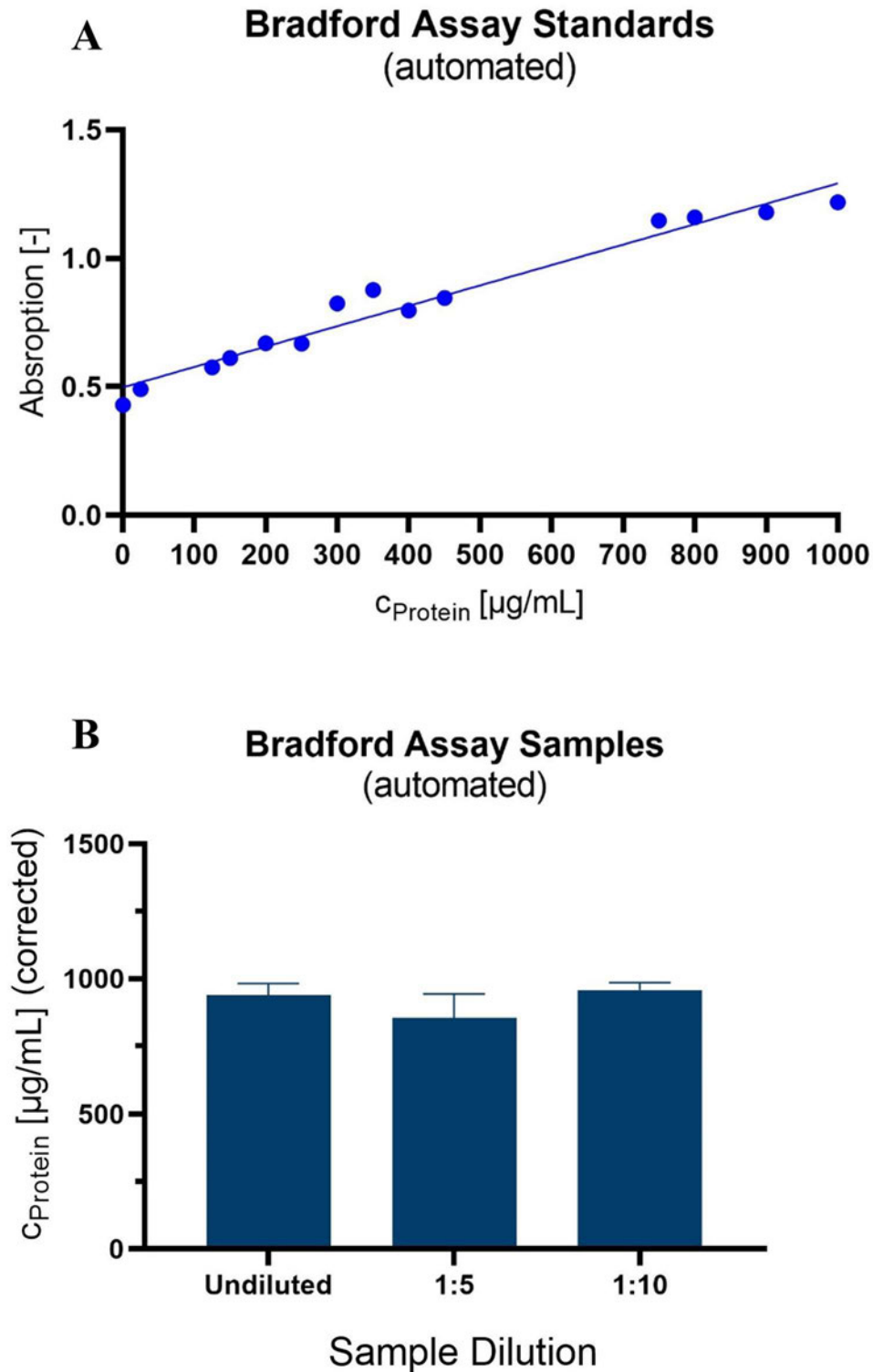
Figure 17: Bradford measurements of the automated assay. (A) Linear regression of the assay standards. (B) Corrected protein concentration of the diluted samples.

The successful automation of the process was confirmed based on the comprehensive data obtained from the replicates and different dilutions, which exhibited low deviation.

5.3. BioLector® cultivation of *K. phaffii*

5.3.1. Determination of carbon source concentration for later POX induction

Before starting with the methanol induction experiments, the best concentration of glycerol or glucose in the batch phase had to be determined. The goal was to achieve a high cell density while still maintaining good reproducibility. Because of its lower price glycerol is generally considered more a feasible carbon source at an industrial scale. Hence, more glycerol conditions were tested to get a more detailed insight of the growth behaviour of the POX12 strain. The experimental conditions for glycerol ranged from 5 g/L to 50 g/L in increments of 5 g/L, while for glucose, the conditions varied from 10 g/L to 50 g/L with increments of 10 g/L.

In the first experiment, the *K. phaffii* POX12 strain was cultivated with different glycerol and glucose concentrations as explained in chapter 4.1.3.1. Results of the backscatter and dissolved oxygen of the cultivation with glycerol can be seen in Figure 18. Figure 19 shows the results of the fermentation with glucose. The pH-value for both fermentations are displayed in Figure 19 (C).
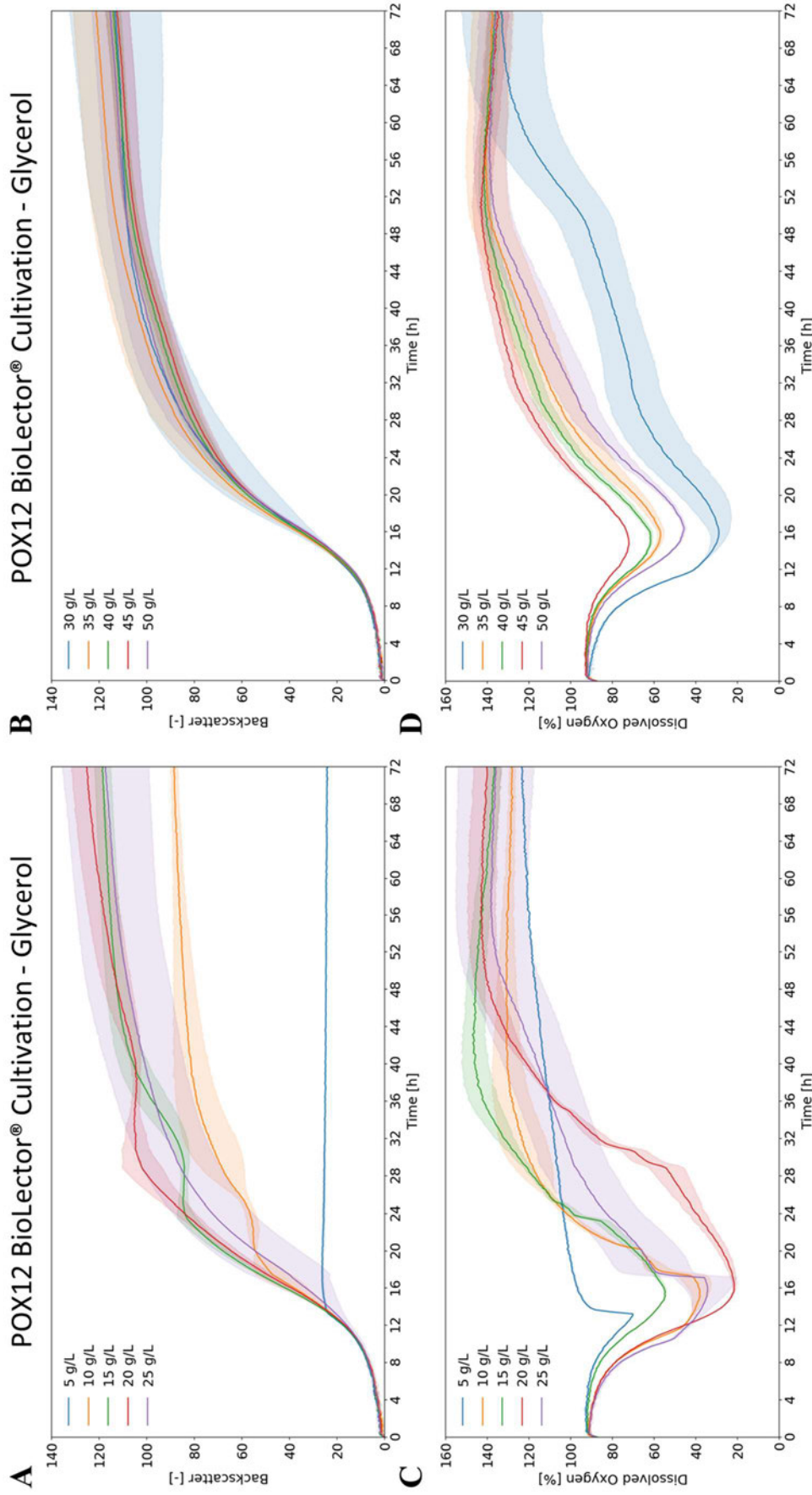
Figure 18: *K. phaffii* POX12 cultivation to determine the best glycerol concentration for BioLector fermentation. (A) Fermentation with glycerol from 5 g/L to 25 g/L. (B) Fermentation with glycerol from 30 g/L to 50 g/L. (C) & (D) Corresponding dissolved oxygen values. For each condition 3 biological replicates were conducted.
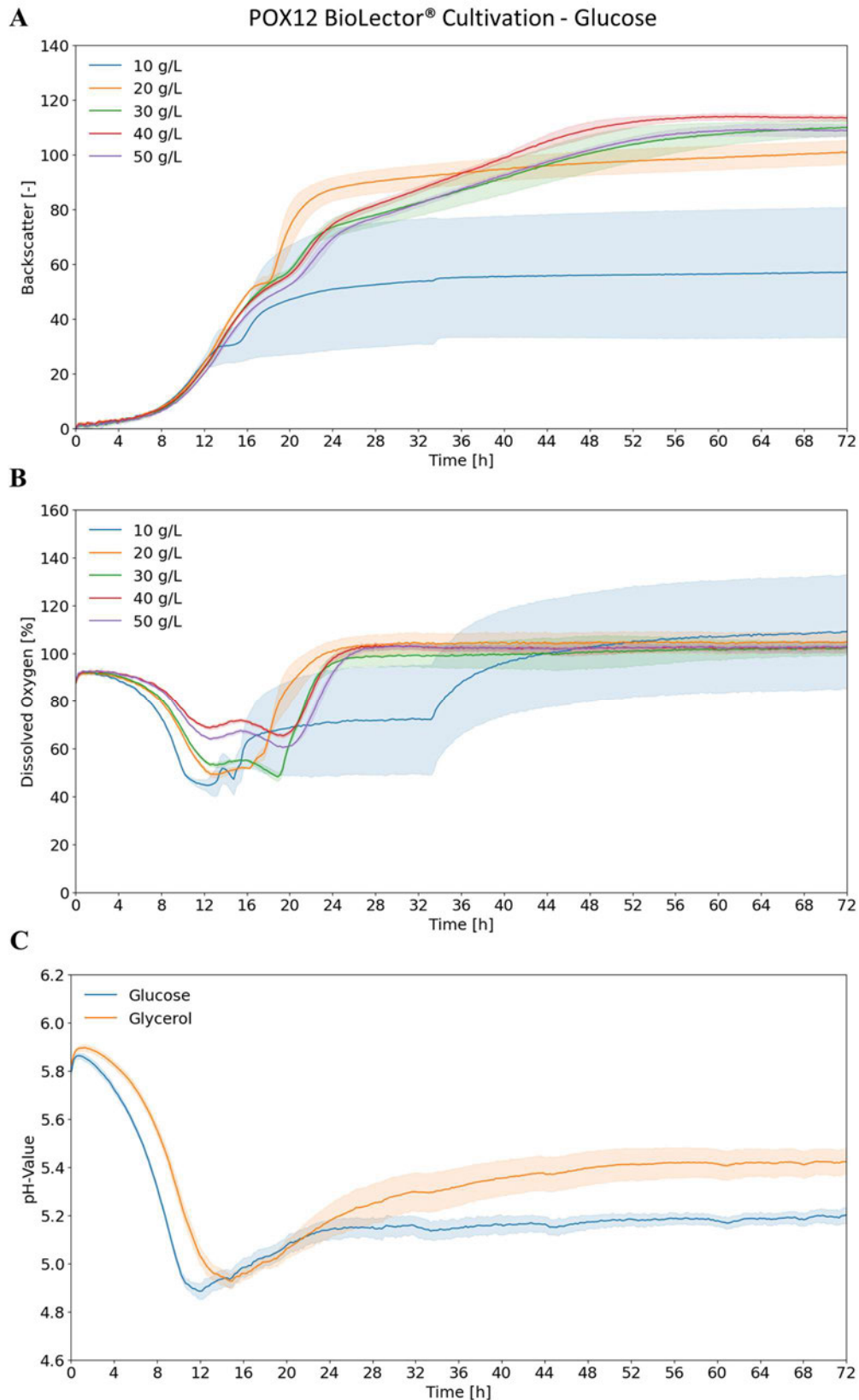
Figure 19: *K. phaffii* POX12 cultivation with different glucose concentration for comparison with glycerol fermentation. For each condition 3 biological replicates were conducted. Cultivation parameters: 1000 rpm shaking frequency, 85 % humidity control and 30 °C temperature. (A) Backscatter values of the fermentation with glucose. (B) Corresponding dissolved oxygen values. (C) pH-Values for the fermentation with glycerol and glucose.

In Figure 18 (A) one can see that the higher the glycerol concentration, the later the plateau in backscatter signal is reached. For the cultivations with 10, 15 and 20 g/L glycerol, a second growth phase is visible, which begins later as the concentration of the carbon source increases. The corresponding dissolved oxygen values (C) first show a decreasing trend and then increase at around t = 16 h. For fermentations with glycerol between 30 g/L and 45 g/L , a higher glycerol concentrtaion led to smaller decrease in DO until t = 16 h. Conversely, for cultivations with higher glycerol concentrations (B), a second increase in cell growth is not visible. The graphs all show a similar trend, however, the deviation between replicates is considerably higher in comparison to the fermentations with glycerol concentrations less than 25 g/L. The corresponding dissolved oxygen values (D) show that, except of the cultivation with 50 g/L glycerol, the higher the C-source concentration the faster the decrease of the graph trends. Similar to the fermentation with lower glycerol concentrations, the dissolved oxygen increases at around t = 16 h.

In Figure 19 (A), the results demonstrate that all fermentation conditions lead to a secondary increase in cell growth. However, the 10 g/L glucose condition exhibits high deviation within the replicates compared to all other glucose concentrations. Among the glucose conditions of 30 g/L, 40 g/L, and 50 g/L, similar backscatter trends are observed, with 40 g/L glucose condition displaying the highest value at the end of the cultivation. In (B) one can see that for all conditions greater than 10 g/L glucose the DO reaches 100 % at around t = 26 h after an initial decrease. The pH-values (C) for all glycerol and glucose fermentation conditions indicate low deviations between different concentrations of the same carbon source. The pH-values decrease and stabilize after a slight increase, with glucose fermentation reaching stability faster (at around pH = 5.1), while glycerol fermentation shows a stronger increase in pH (to around pH = 5.4).

Subsequently, the experiment was repeated with the WT of *K. phaffii* with equal conditions to the POX12 strain cultivation. The purpose was to observe possible differences in the growth behaviour between those two strains, see Figure 20.
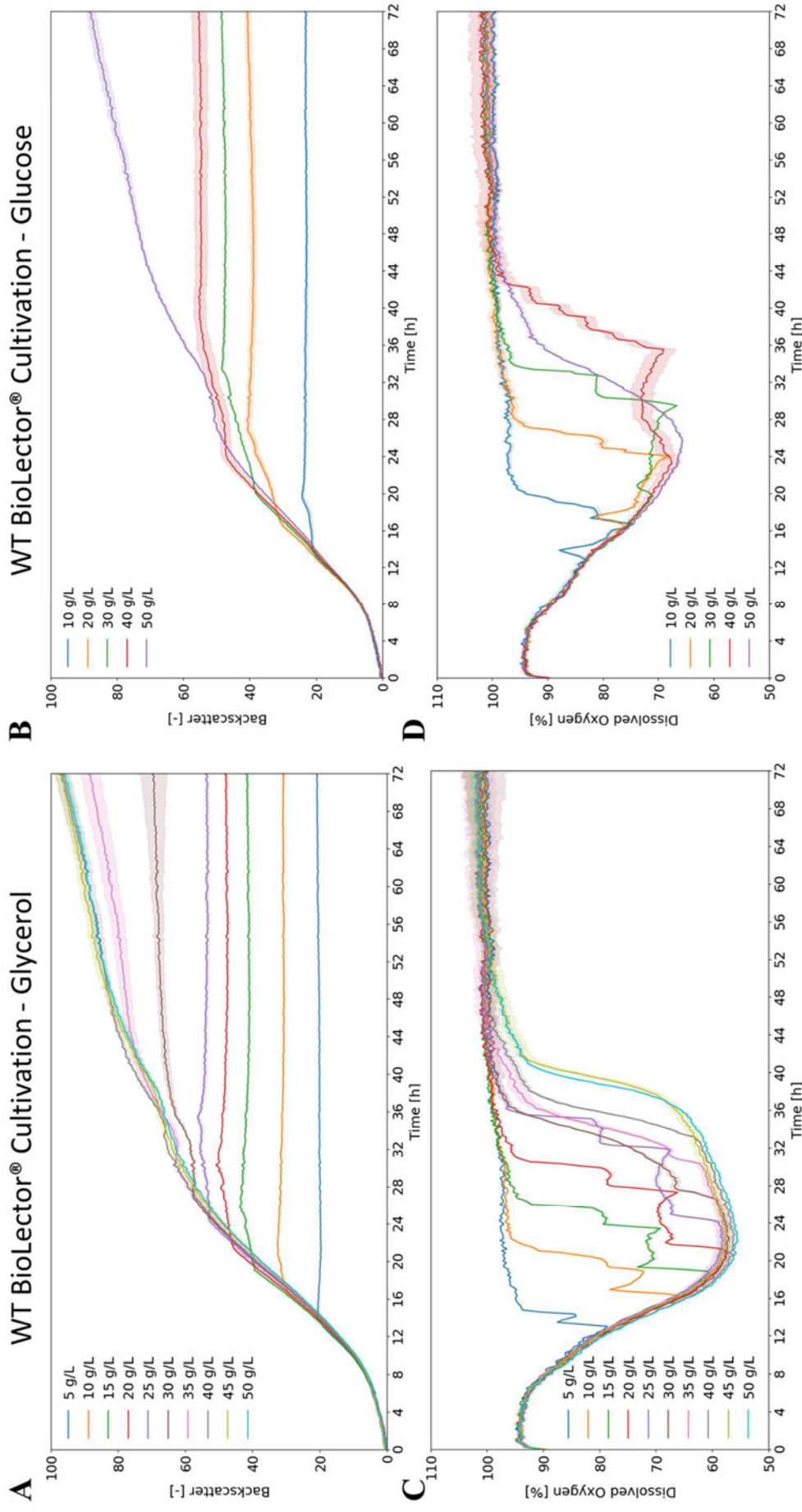
Figure 20: *K. phaffii* WT cultivation with different C-source concentrations for comparison with the POX12 strain. For each condition 3 biological replicates were conducted. Cultivation parameters: 1000 rpm shaking frequency, 85 % humidity control and 30 °C temperature. (A) Fermentation with glycerol from 5 g/L to 50 g/L in increments of 5 g/L. (B) Fermentation with glucose from 10 g/L to 50 g/L in increments of 10 g/L. (C) & (D) Corresponding dissolved oxygen values.

The results in Figure 20 (A) and (B) show, that the higher the concentration of the respective carbon source, the later a backscatter plateau is reached, resulting in higher backscatter values at the end of the cultivation. For cultivations with a higher concentration than 30 g/L of glycerol or glucose, a plateau is not reached at the end of the fermentation. The data of the dissolved oxygen values in (C) and (D) are coherent to the backscatter values. Except for the cultivation with 50 g/L glucose, the lower the carbon source concentration, the faster the oxygen values again increase to 100 %. Overall, the data in this experiment display significantly lower deviation within replicates in contrast to the cultivation with the POX12 strain.

5.3.2.   Methanol feeding for POX production

Based on the findings presented in Figure 18, which indicate significant variation in replicates with carbon concentrations exceeding 25 g/L, and no increase in biomass beyond 25 g/L, subsequent cultivations were conducted using 25 g/L of glycerol or glucose, respectively.

In a first experiment, production of POX was attempted by manually pulsing methanol. The added methanol solutions had a concentration of 400 g/L. Different voluminal were pipetted into the respective cells to reach methanol concentrations of 0 g/L, 1 g/L, 2 g/L, 3 g/L, 4 g/L and 8 g/L and were added after 45 h, 47 h, 49 h, 51 h, 53 h as well as after 69 h and 71 h of cultivation time. The data of the cultivation is displayed in Figure 21. Since the different methanol concentrations showed no differences in the growth behaviours, DO or pH values, the mean of all conditions were plotted together.
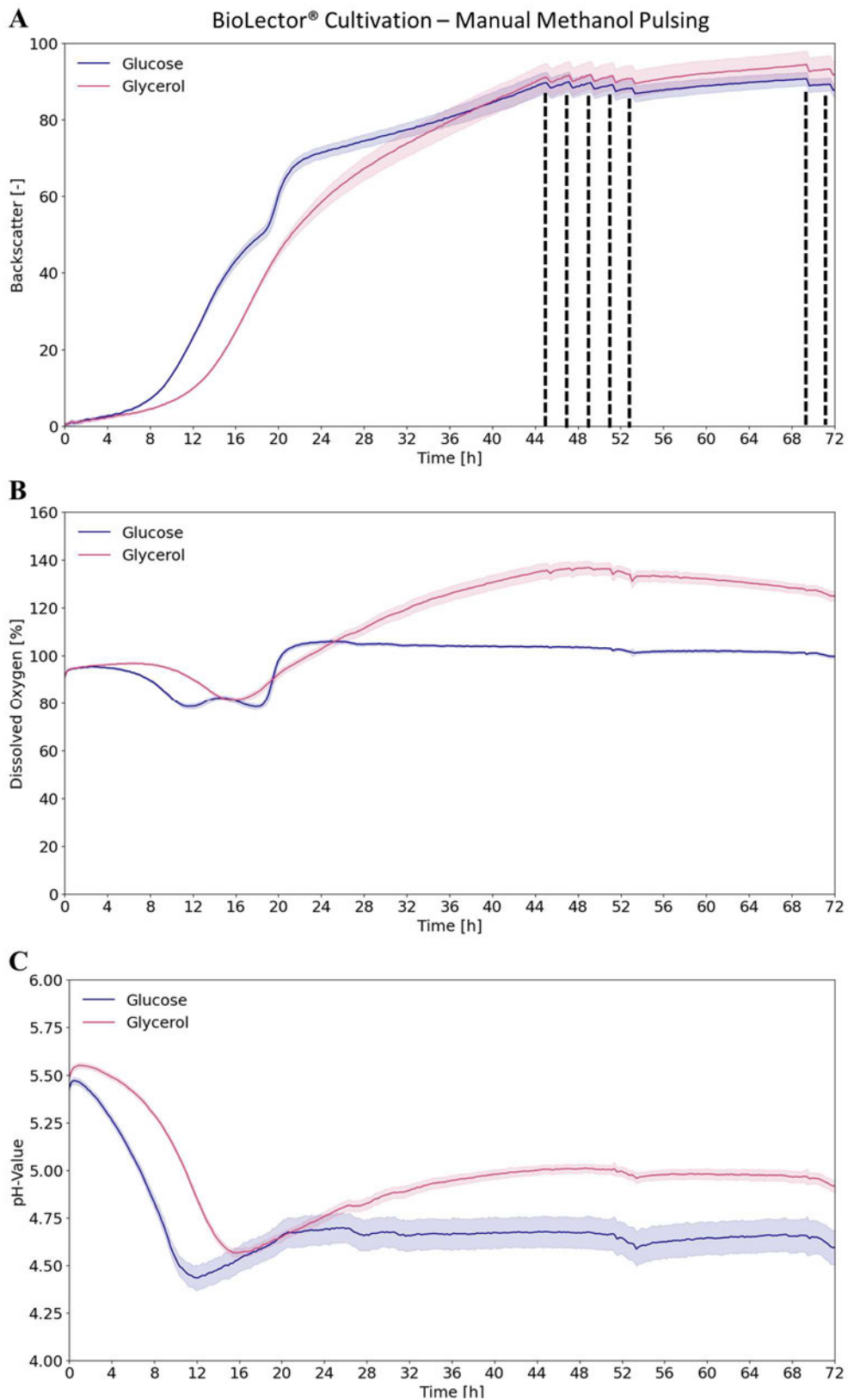
Figure 21: Cultivation data for the manual methanol pulsing for POX expression. All conditions were measured in biological quadrulpicates with 25 g/L of glycerol or glucose, respectively. Cultivation parameters: 1000 rpm shaking frequency, 85 % humidity control and 30 °C temperature. (A) Backscatter data of the cultivation is shown. The dashed vertical lines mark the time when 20 μL of the respective methanol solution was pulsed to the dedicated wells. (B) & (C) The respective DO and pH values are shown.

In Figure 21 (A) one can see that the cultivations with 25 g/L glucose exhibit a faster increase in backscatter value than cultivations with 25 g/L glycerol. Additionally, the cells cultivated with glycerol show a second growth phase at approximately 19 hours of cultivation. At around 40 hours of cultivation, the backscatter values of all fermentation conditions converge, with glycerol cultivations showing slightly higher values at the end. The dissolved oxygen data (B) shows that for the fermentations with glucose after initial decrease, a first slight increase can be seen. Then, a second increase is visible, leading to stable values of 100 % dissolved oxygen after around 22 hours. The cultivations with glycerol as carbon source also display an initial decrease of dissolved oxygen. The value then increases and exceeds 100 %, and then decreases again at t = 50 hours. The graphs for the pH-values (C) show similar trends to the graphs of the dissolved oxygen values by first showing a decrease followed by an increase. The fermentations with glucose show stable values of pH 4.7 after 20 hours. The fermentations with glycerol show a slower and lesser decrease of pH followed by a higher increase.

Following the BioLector® fermentation, the Bradford and ABTS assays were conducted. However, no substantial protein concentration or enzymatic activity was observed. The assays were repeated with undiluted samples, also resulting in no measurable signals. Therefore, this data is not shown.

In the next experiment, the strategy of methanol addition was changed. Here, a constant methanol feed was applied to mediate the POX expression. This constant feed was achieved by using the microfluidic method (see chapter 4.1.4.2). In addition, a fed-batch cultivation was conducted to increase the cell count for a greater chance of POX production (see chapter 4.1.2.1). Thus, the cultivation was conducted with an initial glycerol concentration of 25 g/L, then a fed-batch with a total fed glycerol concentration of 100 g/L glycerol was applied after finally feeding a 70 %, 50 %, 30 % and 0 % solution of methanol. For each condition, 8 biological replicates were conducted. The fermentation data can be seen in Figure 22.
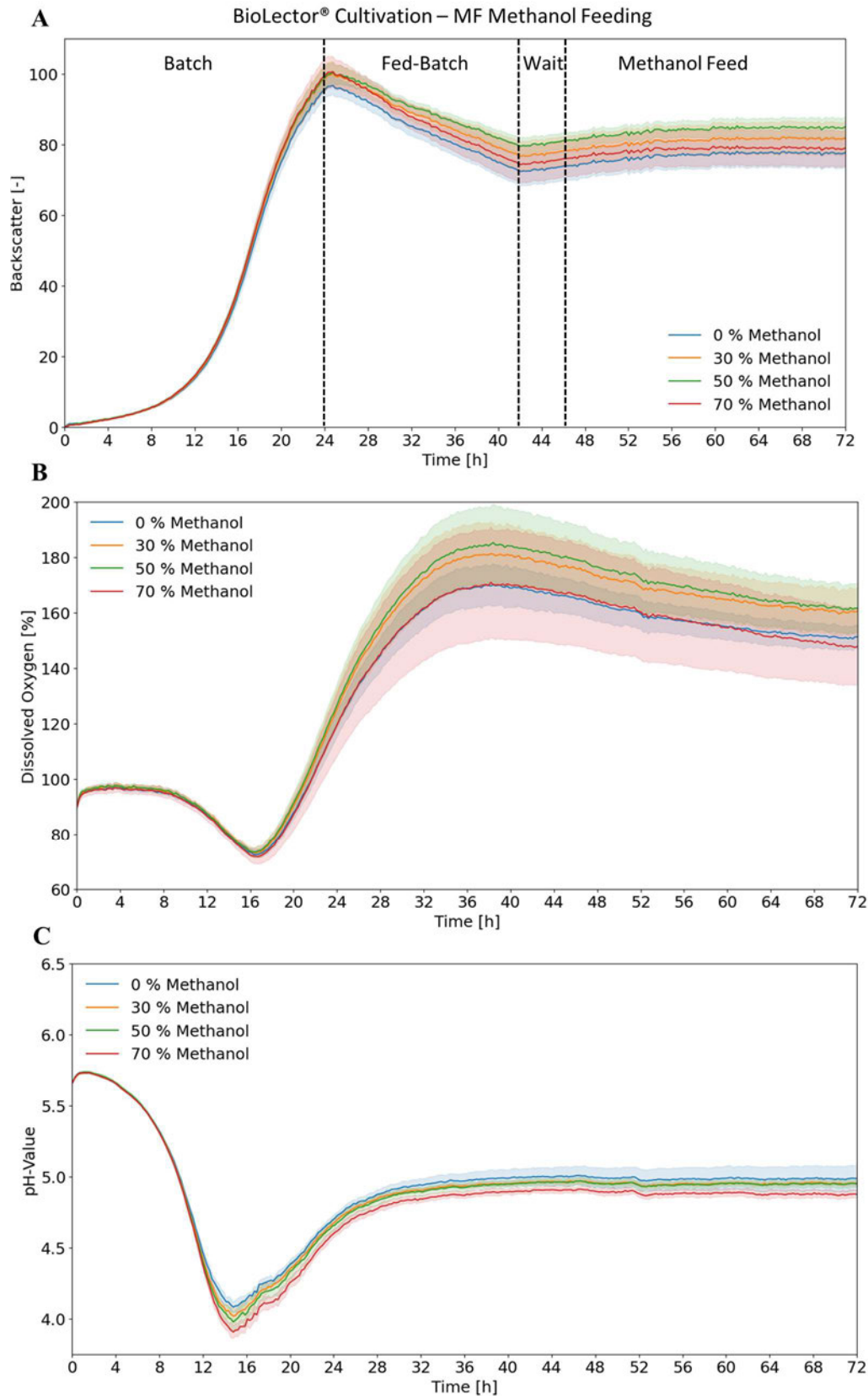
Figure 22: Cultivation data for the MF methanol feed for POX expression. Samples were measured as 8 biological replicates. Here, the glycerol concentration was 25 g/L. Cultivation parameters: 1000 rpm shaking frequency, 85 % humidity control and 30 °C temperature. (A) Backscatter data of the cultivation is shown. Vertical lines mark the different phases of the fermentation. (B) & (C) The corresponding DO and pH values are shown.

Figure 22 (A) shows that the backscatter increases in the batch phase, then decreases during the fed-batch phase until reaching a stable value for the rest of the cultivation. After an initial stable value, the dissolved oxygen values (B) decrease until approximately 17 hours of cultivation. Hence, the dissolved oxygen increases up until 38 hours and then slightly decrease again. The pH values displayed in (C) first drops to approximately pH 4. Afterwards, the pH increases and reaches a stable value of about 4.9.

Overall, all cultivations display similar progressions, independent from the added methanol concentration. Except of the dissolved oxygen data, the backscatter and pH data show low abbreviation within the eight replicates.

Again, the automated Bradford and ABTS assays were conducted with this cultivation samples. However, both assays again showed no detectable levels of protein concentration or enzymatic POX activity, even when conducting the assays with undiluted samples. Hence, this data is not shown.

6. Discussion

The aim of this study was the development of an automated, microcultivation and analytical workflow for screening of peroxygenase producing *K. phaffii* strains. Therefore, a robust and automated analysis workflow needed to be created first. Hence, the ABTS assay was chosen to determine the enzymatic activity of POX, the target protein.

The first manually pipetted assay showed, that a 1:50 dilution is too high to measure the enzymatic activity. The 1:5 dilution however resulted in promising absorbance values. Thus, all following ABTS assays were conducted with 1:5 diluted samples.

Figure 11 displays a relatively high deviation between replicates of the first automated ABTS assay which indicated room for improvement regarding the newly created workflow. In Figure 12 (A) one can see that the right plate side features higher absorptions than the left plate side. Note, that the layout of the FlowerPlate® is transferred twice into the MTP plate with multidispense steps. That means, that the sample in well A1 from the FlowePlate® is first pipetted into well A1 and then well A7 of the MTP, *etc* (see Figure 10). Thus, it is safe to assume that the pipetting layout of the LiHa in this workflow leads to a larger pipetting volume in the second dispensing step, when dispensing the samples. The reason for this lies in the LiHa pipetting mechanism. This issue is depicted in Figure 23. The liquid transfer process involves pneumatic manipulation of the system liquid (blue) within the steel needles. To prevent mixing between the system and the sampled liquid, a trailing air gap (purple) and a leading air gap (yellow) within the needles separate the liquids. Additionally, a sample trailing air gap (green) follows the sample (orange) to prevent any liquid loss from the needles during the pipetting process. However, there is no additional air gap when aspirating a larger volume of liquid which is meant to be dispensed stepwise. The sample trailing air gap is dispensed with the first multidispense step. In the second multidispense step, the dead volume of this air gap is not taken into account, resulting is a larger dispensed volume. Thus, the pipetting accuracy decreases, and the dispensed volumes of the multi-dispense steps can differ, especially with lower volumes. Hence, multi-dispense steps were eliminated and replaced with single pipetting steps. Adding more washing steps to the workflow rebuilds the air gaps, resetting the pipetting accuracy.
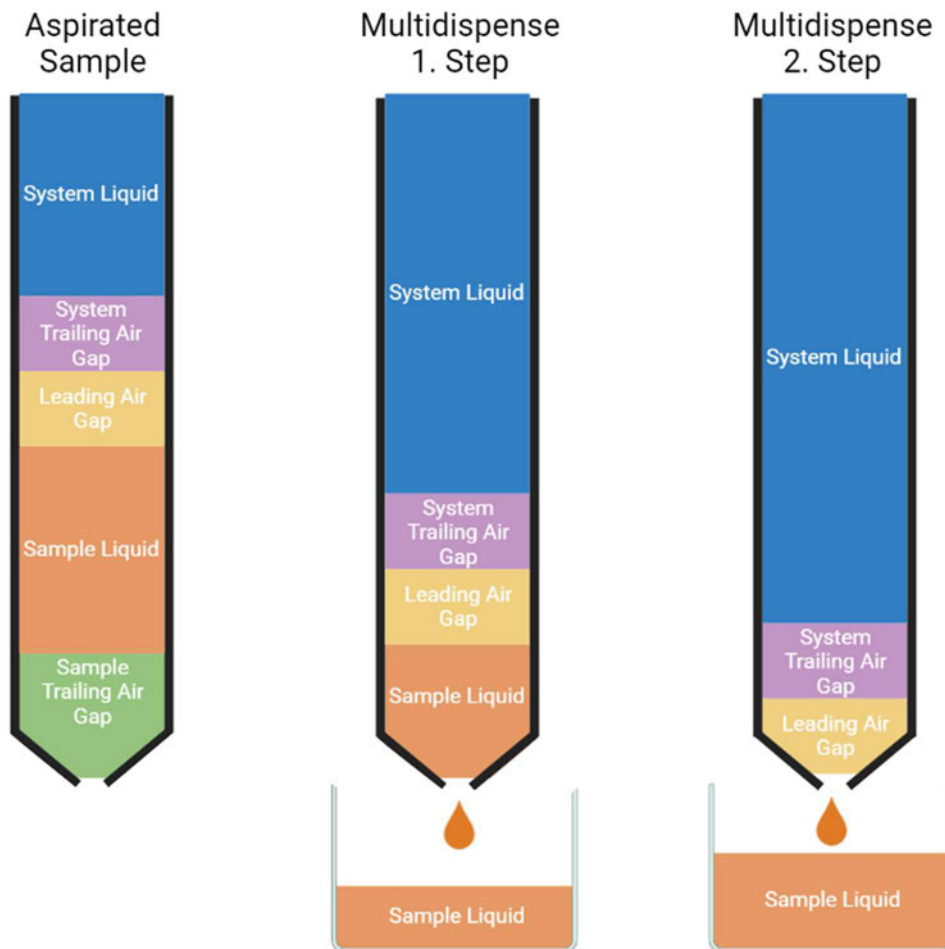
Figure 23: Depiction of the issue of multi-dispense pipetting of the LiHa.

The adapted assay workflow showed that the observed plate effect was eliminated by the single pipetting steps. Now, the enzymatic POX activity needed to be calculated. One variable in Equation 2 is the change in absorption per time ($\frac{\Delta A}{\Delta t}$). Thus, the timespan Δt needed to be determined. With linear regression analysis, the timespan was determined to $\Delta t = 8$ min, with the criteria of a coefficient of determination greater than 0.99. With this the enzymatic activity was calculated to $U_{mean} = 0.065 \; \frac{\mu mol}{mL \cdot min}$, and the average percentage deviation between replicates to $U_{avg\%D} = 4.5\,\%$, thus, satisfying the goal of $U_{avg\%D} < 10\,\%$.

Next, the sensitivity of the assay was studied by measuring the POX activity of a sample with different dilutions. Since the same sample for this and the previous ABTS assay was used the same enzymatic activity for the corrected measurements was expected. Although

the ABTS results show low abbreviation within the same assay, the values are lower than in the previous one. This might be due to different sample handling before the assay. The used samples were frozen and had to be defrosted. Here, the thawing time differed by several hours, though, the exact time was not recorded. However, the overall goal of the workflow is to be able to compare different POX strains after a BioLector® cultivation. As long as the samples are treated equally after cultivation this issue should not occur.

When looking at the results in Figure 14 (A), it becomes apparent that the initial absorption at $t = 0$ min varies among the different dilutions. Given that the ABTS assay is a kinetic assay, and all dilutions were measured on a single MTP, the y-axis interceptions, representing the starting points of the absorbance curves, should exhibit minimal differences in their distances on the y-axis. To achieve this, the workflow was once more adjusted.

By dividing the plate in three segments, as displayed in Figure 15, the time between pipetting the assay solution to the samples and measuring each well decreases, which can be seen by the same starting value of absorption for each plate segment. This workflow shows that abbreviations between the plate segments are minimal as well as the average percentage deviation between replicates. For this reason, the automation of the ABTS assay deemed successfully and was completed. This optimization of the assay procedure enables an accurate and precise distinction between different process parameters and strains which is crucial for the overall screening workflow. All following assays were executed using this workflow.

The next step of developing the automation workflow was to establish and automate the Bradford assay to evaluate the protein concentration in the supernatant of the cultivation broth. To begin with, the assay was conducted manually to determine a protein concentration value for later comparison with the automated assay. Figure 16 (A) shows a satisfying determination of the standard curve. The interpolated protein concentration in (B) however, display inconsistent data. Here, a higher dilution led to higher corrected protein concentration values. A reason for this might be the nature of the Bradford standard curve. To interpolate the protein concentration, a simple linear regression was fitted through the values of the standards. Although the typical response curves for BSA progresses like a

saturation curve, here, a linear correlation was assumed. It should be noted that the undiluted sample surpassed the confidence range of the standard curve, leading to an underestimation of the actual protein concentration. Hence, for future estimations of protein concentration, the samples should be measured in different dilutions to assess the best one for this particular sample.

For the automated assay, more BSA standards were implemented to better cover the lower ranges of the assay. Now, samples from a 1 L fermentation were tested. In Figure 17 one can see that although the coefficient of determination of the standard curve (A) is lower than in the previous assay, the corrected protein concentrations (B) show high consistency. Here, samples indicate a protein concentration of $c_{Protein} \approx 1$ µg/mL. Due to this coherent data the automation of the Bradford assay was considered successful.

After the automation of the analytical assays was completed, the optimization of the microcultivation started. The first step was to assess the right concentration of glycerol or glucose in the batch phase, respectively, for later cultivation with POX induction. Hence, the growth behaviour of *K. phaffii* POX12 and the WT was observed during batch fermentation. The data in Figure 18 and Figure 19 showed that for all cultivations with glucose and for cultivations with glycerol up to 25 g/L a second growth phase is visible. This is most likely due to secondary metabolism, which is common in cultivation of *K. phaffii*. This second growth phase can also be seen in the pH trend of the cultivation in Figure 19 (C). First, the pH decreases because of the increasing concentration of acetate, which is a side product of *K. phaffii* [30,31]. During the second growth phase acetate is consumed again, hence, the pH increases slightly [30,31]. For glucose as C-source, the initial decrease is stronger with a subsequent weaker increase compared to fermentations with glycerol. This general trend of the pH is equal for all fermentations of the POX12 strain. In contrast, this second growth phase is not that apparent for the WT which can be seen in Figure 20. While observing the DO data in Figure 19 (B) and Figure 20 (C) and (D), one can see that the DO decreases while the backscatter increases. Here, a higher cell titre led to a higher oxygen uptake, hence the DO value decreased. When the respective backscatter data reached a plateau, the DO values increased again, until reaching 100 % DO. This is because the cells switched from a growth metabolism to a maintenance metabolism which requires a lower oxygen amount. However, one striking difference to this can be seen in

Figure 18 (C) and (D), the DO data for the POX12 cultivation with glycerol as carbon source. Here, all cultivations exceeded 100 % DO. In fact, this phenomenon can be seen for all cultivations where POX12 was cultivated with glycerol. Given the fact that the DO value cannot surpass 100 %, these measurements must be considered erroneous readings. It can be assumed that a by-product of glycerol metabolism causes the DO optode of the FlowerPlate® to be corrupted. This hypothesis is supported by the fact that 1 L fermentations of the POX12 with glycerol do not lead to similar observations, since DO probes are more resilient than the optodes on the FlowerPlate®. Henceforth, when cultivation the POX12 strain with glycerol, the DO data can only be considered a rough estimate of the actual DO value of the fermentation.

Generally, the deviation between replicates is relatively low in the WT fermentation compared to the other two. This demonstrates that the modifications of the POX12 strain affect the growth behaviour of the organism. Based on these findings a glycerol and glucose concentration of 25 g/L was determined for the subsequent cultivations.

To induce the POX expression in the *K. phaffii* POX12 strain, methanol induction is needed. The methanol induction is already established in shake flask and lab scale cultivation of 1 L bioreactors. For high throughput screening of other strains, the establishment in microscale is crucial. In a first experiment, methanol was induced by manually pulsing it into the cultivation wells. In Figure 21 the results of this cultivation can be seen. The overall fermentation data is coherent with the previous cultivations *i.e.*, the second growth phase for the cultivation with glucose or the DO data of glycerol fermentations exceeding 100 %. The fast and short decreases in the backscatter data in Figure 21 (A) are due to the methanol pulses. Since methanol was diluted with distilled water, adding the solution to the wells increases the cultivation volume and hence, led to decreases in the backscatter data.

After 72 hours the cultivation was completed, and the cell suspension was immediately processed further to conduct the Bradford and ABTS assays. None of the cultivation conditions led to a recordable value of POX activity or protein concentration. Thus, the methanol pulsing did not lead to induce to expression of POX. One reason for this could be, that the glycerol or glucose, respectively, was not entirely used up by the microorganisms

at the time the methanol was introduced to the yeast. This can be seen in Figure 21 (A). Here the backscatter data did not reach a clear plateau before the addition of the methanol. As explained, the PDF promotor, which regulated POX production, is highly repressed in the presence of carbon sources other than methanol [19–21,24,25]. Another reason could be the pH value during cultivation. Figure 21 (B) shows, that the initial pH value of 6 decreases and then stabilizes at around 4.7 for cultivations with glucose and 5.0 for glycerol as carbon source. Although *K. phaffii* can grow under a broad pH range of 3 – 7 , pH changes can lead to altered specific growth rates and activation of host cell proteases [32,33]. Hence, it is plausible to consider that the absence of pH regulation during the BioLector® cultivation may have resulted in the degradation of the POX enzyme. A counterargument could be made based on the successful POX induction in shake flask cultivations, despite the absence of pH regulation. However, it is worth noting that the shake flask cultivations utilize BMD1 (Table 6) and BMM10 (Table 7) media, which exhibit a strong buffer effect due to the presence of KPI. Consequently, the pH shift experienced during shake flask cultivations might be relatively low compared to BioLector® cultivation, potentially preserving the integrity of the POX enzyme.

Another possible explanation for the low POX activity could be attributed to a low cell mass in the microbioreactors, which might not have been sufficient to produce a detectable concentration of POX for either of the assays. This can be observed in Figure 21 (C), DO data did not decrease while the backscatter increased. Typically, a higher cell concentration results in increased oxygen uptake, which would be reflected in lower DO values.

To address the possible issue of low cell mass and improve the chances of POX expression, two key adaptations were implemented for the final cultivation. Firstly, a fed-batch cultivation strategy was employed to promote higher cell counts, consequently increasing the number of cells capable of secreting POX after expression. Secondly, a continuous methanol feed was introduced to have a stronger lever on the MUT pathway, which is crucial to provide carbon for the protein biosynthesis of POX.

The results in Figure 22 show that the batch phase led to similar data as the previous cultivation. When the fed-batch phase starts, the backscatter data decreases and

continuous to decrease until the fed-batch phase ends. Because the decrease start immediately after the feed starts, it is safe to assume that the dilution of the cultivation broth via the feed solution is stronger than the increase of cell count. In general, the backscatter, DO and pH data show similar values and trends for the different concentrations of the methanol feeds. Hence, the different feeds have no greater impact on the cultivation itself.

After this fermentation, the analytical assays were performed. Once again, no measurable signals were detected for either of the assays. This negative outcome indicates that the previous challenges in detecting protein concentrations and POX activity persisted, despite the modifications made to enhance cell mass and improve POX expression. As before, the samples were also measured undiluted, in case low protein concentrations or POX activity could be detected.

To conclude this work, it is safe to say that the analytical part of the workflow automation is successfully completed. The assays show to be reliable and produce reproducible data. Especially the implemented ABTS assay demonstrated robustness and consistency in determining the enzymatic activity of POX, providing a critical parameter for the screening process. The automation of this assay workflow was achieved through optimization, addressing issues such as pipetting accuracy and plate effects. The POX expression via methanol induction during BioLector® microcultivations proved to be more challenging than anticipated. The inability to observe significant signals suggests that the protein concentrations and POX activity were still below the detection limits of the assays utilized. Interestingly, experiments conducted by colleagues using 1 L fed-batch cultivations with the similar parameters have shown detectable protein concentrations and POX activities. Despite the challenges encountered, the completion of the analytical part of the workflow automation provides a solid foundation for future research and optimization.

Overall, this study has made significant progress in establishing a reliable workflow for the screening of POX producing *K. phaffii* strains. Moving forward, further investigation is required to overcome the challenges associated with POX induction, paving the way for future advancements in this field of research.

7. Outlook

Despite the efforts made to enhance cell mass and improve POX expression through adjustments such as fed-batch cultivation and continuous methanol feed, no significant signals were observed in the assays. To overcome this issue, several actions can be taken. For one, lower concentrations of glycerol should be tested in combination with methanol induction. The current concentration of 25 g/L glycerol may lead to overflow metabolism and repression of the PDF promoter. By reducing the glycerol concentration, POX expression could be promoted. Additionally, instead of conduction a fed-batch fermentation, a batch fermentation can be performed to use one reservoir well of the MF Flower-Plate® for pH control. By maintaining a stable pH throughout the fermentation, any potential decrease in POX activity caused by pH shifts can be mitigated. Lastly, when conducting a fed-batch fermentation, it is advisable to consider a longer waiting phase than the current 4 hours. Extending the waiting phase allows for the complete consumption of the carbon source, ensuring optimal activation of the PDF promoter and potentially enhancing POX expression. Moreover, it would also be possible to cultivate without adding methanol and instead utilize a limited glycerol feed. This approach could result in partial derepression of the PDF promoter and potentially lead to POX expression.

By implementing these actions, it is anticipated that the challenges associated with achieving detectable POX activity can be addressed. It is important to carefully evaluate and optimize each parameter to enhance the expression and activity of the POX enzyme in the BioLector® microcultivation system.

Moving forward, once the current workflow optimization is successfully completed and the desired POX expression is achieved, different POX strains can be tested. By comparing the results obtained from these screenings, the most promising strains can be identified based on their performance in terms of POX expression. Additionally, more key performance indicators like total biomass yield, product yield and product activity can be compared. This comprehensive evaluation allows for the identification of strains that exhibit not only high POX production levels but also demonstrate superior POX activity. By considering multiple metrics with the ABTS and Bradford assay, a more thorough assessment can be conducted to select the most promising strains for further development.

Following the identification of the most promising strains, the next step would be to validate their performance through scale-up fermentations. Initially, a 1 L scale fermentation can be performed to assess the strain's behaviour and productivity in a larger volume. This step helps to ensure that the strain performs consistently and reliably at a larger scale. Once the 1 L scale fermentation is successfully completed, the next stage would involve conducting industrial-scale cultivations. These large-scale fermentations would aim to further validate the strain's performance, productivity, and overall suitability for industrial production.

Regarding the choice of carbon source, glycerol is favoured over glucose in future industrial applications because of several advantages. One notable benefit of using glycerol as a carbon source over glucose is its lower price point, primarily attributed to its status as a by-product of biodiesel production. The availability of glycerol as a waste product contributes to its economic viability and cost-effectiveness in bioprocesses. Moreover, utilizing glycerol as a carbon source aligns with sustainability goals by repurposing a waste material and reducing overall waste generation [34].

In addition to the mentioned parameters, there are numerous other factors that can be optimized to enhance the identification of the optimal strain. For instance, adjustments to the pH in the beginning and during cultivation can be explored. Furthermore, the composition of the BioLector® cultivation and feed media can be fine-tuned to improve pH buffering and mitigate observed pH shifts. The methanol induction method is also a valuable aspect to optimize. Various strategies, such as implementing a DO-triggered start for methanol addition or employing frequent methanol pulsing via the LiHa, can be investigated to enhance POX expression and productivity.

By systematically testing different strains, validating their performance through scale-up fermentations, and eventually moving to industrial-scale cultivations, it becomes possible to identify and select the most promising POX strain for potential industrial applications, eventually replace cobalt curing with a biotechnologically produced POX enzyme in the future.

8. References

1. Bareither, R. & Pollard, D. A review of advanced small-scale parallel bioreactor technology for accelerated process development: current state and future need. *Biotechnology progress* **27,** 2–14; 10.1002/btpr.522 (2011).

2. Long, Q. *et al.* The development and application of high throughput cultivation technology in bioprocess development. *Journal of biotechnology* **192 Pt B,** 323–338; 10.1016/j.jbiotec.2014.03.028 (2014).

3. Fink, M., Cserjan-Puschmann, M., Reinisch, D. & Striedner, G. High-throughput microbioreactor provides a capable tool for early stage bioprocess development. *Scientific reports* **11,** 2056; 10.1038/s41598-021-81633-6 (2021).

4. Gupta, S. K., Dangi, A. K., Smita, M., Dwivedi, S. & Shukla, P. Effectual Bioprocess Development for Protein Production. In *Applied Microbiology and Bioengineering* (Elsevier2019), pp. 203–227.

5. Bhambure, R., Kumar, K. & Rathore, A. S. High-throughput process development for biopharmaceutical drug substances. *Trends in biotechnology* **29,** 127–135; 10.1016/j.tibtech.2010.12.001 (2011).

6. Hemmerich, J., Noack, S., Wiechert, W. & Oldiges, M. Microbioreactor Systems for Accelerated Bioprocess Development. *Biotechnology journal* **13,** e1700141; 10.1002/biot.201700141 (2018).

7. Dietzsch, C., Spadiut, O. & Herwig, C. A fast approach to determine a fed batch feeding profile for recombinant Pichia pastoris strains. *Microbial cell factories* **10,** 85; 10.1186/1475-2859-10-85 (2011).

8. BoostLab6-1: EnzyPol - Enzymatische Alternativen für KobalttrocknerAACHEN UNIVERSITY bio4matpro - Deutsch (2022).

9. Chartoff, R. P., Cho, J. & Carlin, P. S. Morphology and mechanical properties of rubber modified aromatic-ether bismaleimide matrix resins. *Polym. Eng. Sci.* **31,** 563–566; 10.1002/pen.760310805 (1991).

10. Jansen, J. F. *et al.* Cobalt Replacement in Unsaturated Polyester Resins; Going for Sustainable Composites. *Macromol. Symp.* **329,** 142–149; 10.1002/masy.201200102 (2013).

11. Kathrin Witsch. Die schwierige Suche nach der kobaltfreien Batterie. *Handelsblatt* (2020).

12. Susanne Preus, Henning Peitsmeier, Carsten Germis. An Kongo führt kein Weg vorbei. *Frankfurter Allgemeine Zeitung* (2020).

13. Rahimpour Golroudbary, S., Farfan, J., Lohrmann, A. & Kraslawski, A. Environmental benefits of circular economy approach to use of cobalt. *Global Environmental Change* **76,** 102568; 10.1016/j.gloenvcha.2022.102568 (2022).

14. Singh, R., Kumar, M., Mittal, A. & Mehta, P. K. Microbial enzymes: industrial progress in 21st century. *3 Biotech* **6,** 174; 10.1007/s13205-016-0485-8 (2016).

15. Conesa, A., Punt, P. J. & van den Hondel, C. A. M. J. J. Fungal peroxidases: molecular aspects and applications. *Journal of biotechnology* **93,** 143–158; 10.1016/s0168-1656(01)00394-7 (2002).

16. Hammel, K. E. & Cullen, D. Role of fungal peroxidases in biological ligninolysis. *Current opinion in plant biology* **11,** 349–355; 10.1016/j.pbi.2008.02.003 (2008).

17. Nakayama, T. & Amachi, T. Fungal peroxidase: its structure, function, and application. *Journal of Molecular Catalysis B: Enzymatic* **6,** 185–198; 10.1016/S1381-1177(98)00119-2 (1999).

18. Hofrichter, M. & Ullrich, R. Oxidations catalyzed by fungal peroxygenases. *Current opinion in chemical biology* **19,** 116–125; 10.1016/j.cbpa.2014.01.015 (2014).

19. Fischer, J. E., Hatzl, A.-M., Weninger, A., Schmid, C. & Glieder, A. Methanol Independent Expression by Pichia Pastoris Employing De-repression Technologies. *Journal of visualized experiments : JoVE*; 10.3791/58589 (2019).

20. Garrigós-Martínez, J. *et al.* Bioprocess performance analysis of novel methanol-independent promoters for recombinant protein production with Pichia pastoris. *Microbial cell factories* **20,** 74; 10.1186/s12934-021-01564-9 (2021).

21. Vogl, T. *et al.* Orthologous promoters from related methylotrophic yeasts surpass expression of endogenous promoters of Pichia pastoris. *AMB Express* **10,** 38; 10.1186/s13568-020-00972-1 (2020).

22. Eck, A. *et al.* Improved microscale cultivation of Pichia pastoris for clonal screening. *Fungal biology and biotechnology* **5,** 8; 10.1186/s40694-018-0053-6 (2018).

23. Holmes, W. J., Darby, R. A., Wilks, M. D., Smith, R. & Bill, R. M. Developing a scalable model of recombinant protein yield from Pichia pastoris: the influence of culture conditions, biomass and induction regime. *Microbial cell factories* **8,** 35; 10.1186/1475-2859-8-35 (2009).

24. Krainer, F. W. *et al.* Recombinant protein expression in Pichia pastoris strains with an engineered methanol utilization pathway. *Microbial cell factories* **11,** 22; 10.1186/1475-2859-11-22 (2012).

25. Hartner, F. S. & Glieder, A. Regulation of methanol utilisation pathway genes in yeasts. *Microbial cell factories* **5,** 39; 10.1186/1475-2859-5-39 (2006).

26. Schäpper, D., Alam, M. N. H. Z., Szita, N., Eliasson Lantz, A. & Gernaey, K. V. Application of microbioreactors in fermentation process development: a review. *Analytical and bioanalytical chemistry* **395,** 679–695; 10.1007/s00216-009-2955-x (2009).

27. Shuler, M. L. & Kargi, F. *Bioprocess engineering. Basic concepts.* 2nd ed. (Prentice Hall PTR, Upper Saddle River, NJ, 2002).

28. Samorski, M., Müller-Newen, G. & Büchs, J. Quasi-continuous combined scattered light and fluorescence measurements: a novel measurement technique for shaken microtiter plates. *Biotechnology and bioengineering* **92,** 61–68; 10.1002/bit.20573 (2005).

29. m2p-labs GmbH. Technical Data Sheet: FlowerPlate® (48 well MTP, fl ower).

30. Cereghino, G. P. L., Cereghino, J. L., Ilgen, C. & Cregg, J. M. Production of recombinant proteins in fermenter cultures of the yeast Pichia pastoris. *Current opinion in biotechnology* **13,** 329–332; 10.1016/s0958-1669(02)00330-0 (2002).

31. Inan, M. & Meagher, M. M. The effect of ethanol and acetate on protein expression in Pichia pastoris. *Journal of bioscience and bioengineering* **92,** 337–341; 10.1263/jbb.92.337 (2001).

32. Eck, A. *et al.* Improved microscale cultivation of Pichia pastoris for clonal screening. *Fungal biology and biotechnology* **5,** 8; 10.1186/s40694-018-0053-6 (2018).

33. Cregg, J. M., Vedvick, T. S. & Raschke, W. C. Recent advances in the expression of foreign genes in Pichia pastoris. *Bio/technology (Nature Publishing Company)* **11,** 905–910; 10.1038/nbt0893-905 (1993).

34. Chilakamarry, C. R., Sakinah, A. M. M., Zularisam, A. W. & Pandey, A. Glycerol waste to value added products and its potential applications. *Syst Microbiol and Biomanuf* **1,** 378–396; 10.1007/s43393-021-00036-w (2021).

9. Supplemental information

9.1. Abbreviations

9.2. List of figures

9.3. List of tables

9.4. List of equations

10. Acknowledgements

Ich möchte die Gelegenheit nutzen, um mich bei all den Personen zu bedanken, die mich während meiner Abschlussarbeit unterstützt und begleitet haben.

Zuallererst gilt mein herzlicher Dank Prof. Marco Oldiges, dass er mir die Möglichkeit gegeben hat, meine Abschlussarbeit in seiner Arbeitsgruppe zu schreiben.

Ebenso möchte ich bei Prof. Dr. Gesine Cornelissen für die Erstbetreuung meiner Arbeit bedanken.

Ein ganz besonderer Dank geht an Christian Wagner, der mir während meiner gesamten Zeit sowohl mit fachlicher Kompetenz als auch in persönlicher Hinsicht hervorragend zur Seite stand.

Des Weiteren möchte ich mich bei allen Mitgliedern der Arbeitsgruppe bedanken. Ihre Unterstützung und das gute Arbeitsklima haben dazu beigetragen, dass meine Abschlussarbeit erfolgreich war.

Abschließend möchte ich meiner Familie, insbesondere Bianca, meinen größten Dank aussprechen. Ihre emotionale Unterstützung und ihr konstruktives Feedback waren von großem Wert für meinen Erfolg. Ohne sie wäre die Herausforderung deutlich größer gewesen.

11. Statutory Declaration

I hereby formally declare that the Master thesis with the title "Development of an automated, microcultivation and analytical workflow for screening of peroxygenase producing *K. phaffii* strains" was written independently by myself. I did not use any outside support except for the quoted literature and other sources mentioned in the thesis. Passages and ideas originating from external sources are marked clearly, either literally or analogously. The thesis has not been submitted to any examining authority in the same or similar form and has not been published.

_____

Place, Date

Signature